# Inability to switch from ARID1A-BAF to ARID1B-BAF impairs exit from pluripotency and commitment towards neural crest formation in *ARID1B*-related neurodevelopmental disorders

Luca Pagliaroli[1,#], Patrizia Porazzi[2,#], Alyxandra T. Curtis[1], Chiara Scopa[1], Harald M.M. Mikkers[3], Christian Freund[4], Lucia Daxinger[5], Sandra Deliard[6], Sarah A. Welsh[6], Sarah Offley[6], Connor A. Ott[1], Bruno Calabretta[2], Samantha A. Brugmann[7], Gijs W.E. Santen*[,8], and Marco Trizzino*[,1,9]

**#** = Co-First authors
***** = Co-Senior authors
1) Department of Biochemistry and Molecular Biology, Sidney Kimmel Medical College, Thomas Jefferson University, Philadelphia, PA
2) Department of Cancer Biology, Sidney Kimmel Medical College, Thomas Jefferson University, Philadelphia, PA
3) Department of Cell & Chemical Biology, Leiden University Medical Center, Leiden, The Netherlands
4) LUMC hiPSC Hotel, Dept. Anatomy & Embryology, Leiden University Medical Center, Leiden, The Netherlands
5) Department of Human Genetics, Leiden University Medical Center (LUMC), Leiden 2300, RC, The Netherlands
6) Gene Expression and Regulation Program, The Wistar Institute, Philadelphia, PA
7) Division of Developmental Biology, Department of Pediatrics Cincinnati Children's Hospital Medical Center, Cincinnati, OH
8) Department of Clinical Genetics, Leiden University Medical Center, Leiden, The Netherlands
9) Corresponding author: Marco Trizzino, Department of Biochemistry and Molecular Biology, Sidney Kimmel Medical College, Thomas Jefferson University, 233 S 10th Street, BLSB 826, Philadelphia, PA, 19104. E-mail: marco.trizzino@jefferson.edu

**Abstract**

The BAF complex modulates chromatin accessibility. Specific BAF configurations have functional consequences, and subunit switches are essential for cell differentiation. *ARID1B* and its paralog *ARID1A* encode for mutually exclusive BAF subunits. *De novo ARID1B* haploinsufficient mutations cause a neurodevelopmental disorder spectrum, including Coffin-Siris syndrome, which is characterized by neurological and craniofacial features. Here, we reprogrammed *ARID1B*$^{+/-}$ Coffin-Siris patient-derived skin fibroblasts into iPSCs and modeled cranial neural crest cell (CNCC) formation. We discovered that ARID1B is active only during the first stage of this process, coinciding with neuroectoderm specification, where it is part of a lineage-specific BAF configuration (ARID1B-BAF), which includes SMARCA4 and nine additional subunits. ARID1B-BAF acts as a gatekeeper, ensuring exit from pluripotency and lineage commitment, by attenuating *NANOG*, *SOX2* and thousands of enhancers directly regulated by these two pluripotency factors at the iPSC stage.

In iPSCs, these enhancers are maintained active by an ARID1A-containing BAF. At the onset of differentiation, cells transition from ARID1A-BAF to ARID1B-BAF, eliciting attenuation of the NANOG/SOX2 networks, and triggering pluripotency exit. Coffin-Siris patient cells fail to perform the ARID1A/ARID1B switch and maintain ARID1A-BAF at pluripotency enhancers throughout all stages of CNCC formation. This leads to a persistent and aberrant SOX2 and NANOG activity, which impairs CNCC formation. In fact, despite showing the typical neural crest signature (TFAP2A$^{+}$, SOX9$^{+}$), *ARID1B*-haploinsufficient CNCCs are also NANOG/OCT4-positive, in stark contrast with the *ARID1B*-wt CNCCs, which are NANOG/OCT4-negative.

These findings suggest a connection between *ARID1B* mutations, neuroectoderm formation, and a pathogenic mechanism for Coffin-Siris syndrome.

**Keywords**: BAF, ARID1B, Coffin-Siris, pluripotency enhancers, NANOG, SOX2, neural crest, neuroectoderm

## Introduction

Cell fate commitment is a complex process that requires timely regulation of developmental genes. This phenomenon is mediated by the concerted activity of transcription factors (TFs) and chromatin regulators that modulate the interaction between *cis*-regulatory elements (enhancers, promoters) and RNA Polymerase II to promote gene expression. In this framework, a key role is played by the Brg1/Brm associated factor (BAF) chromatin-remodeling complex. BAF leverages ATP to modulate nucleosome positioning and chromatin accessibility genome-wide[1]. Different configurations of BAF, with context specific functions, have been described, and switches between subunits have been reported to be linked to specific developmental stages[2,3]. All known canonical BAF configurations require the presence of a subunit containing an AT-rich DNA binding domain (ARID). Namely, in the BAF complex this function is carried out by two mutually exclusive subunits: ARID1A and ARID1B[4-6]. Previous studies in mouse embryonic stem cells (mESCs) have identified an ESC-specific configuration of BAF which regulates pluripotency and self-renewal of embryonic stem cells (esBAF)[4-6]. Importantly, the esBAF exclusively incorporates ARID1A and not ARID1B. One of these studies also identified a non-canonical version of BAF (gBAF), which did not contain an ARID subunit and was involved in pluripotency maintenance of mESCs [4].
*De novo* haploinsufficient mutations in the *ARID1B* gene cause a spectrum of neurodevelopmental disorders, ranging from Coffin Siris syndrome to non-syndromic intellectual disability[7-12]. Coffin-Siris syndrome is associated with intellectual disability, specific craniofacial features, growth impairment, feeding difficulties and congenital anomalies such as heart and kidney defects[13]. Although other BAF components may also be mutated in this syndrome, approximately 75% of mutations are in *ARID1B* [11,14,15].
In addition to Coffin-Siris, genome-wide sequencing in unselected cohorts of patients with intellectual disability (ID) shows that *ARID1B* is always in the top-5 of causative genes, explaining about 1% of all ID cases[9,16]. Whereas several studies utilizing murine models recapitulate the neurological phenotypes typical of the *ARID1B*-associated syndromes[17-20], the molecular function of ARID1B in cell fate commitment during human development is still poorly understood.
Several hallmark features of *ARID1B* haploinsufficient individuals, including severe craniofacial, cardiac and digestive system abnormalities, suggest impaired neural crest cell migration as a pathological etiology[12]. Further, *ARID1B* is one of the most commonly mutated genes in neuroblastoma, a pediatric tumor of neural crest origin[21]. Thus, neural crest formation, migration, and differentiation represent suitable models to study the consequences of *ARID1B* mutations. To specifically address the molecular consequences of *ARID1B* haploinsufficient mutations in neural crest formation and development, we reprogrammed skin fibroblasts of two unrelated *ARID1B*$^{+/-}$ Coffin-Siris patients into induced Pluripotent Stem Cells (iPSCs) and used these patient-derived iPSCs to specifically model formation of cranial neural crest cell (CNCC), a multipotent cell population that forms through a neuroectodermal sphere intermediate that eventually give rise to migratory CNCCs.
Herein, we report the discovery of a lineage specific BAF configuration, containing ARID1B, SMARCA4 and seven additional subunits (ARID1B-BAF). In line with findings indicating that the esBAF and the gBAF do not contain ARID1B[4-6], we demonstrate that *ARID1B* mutations do not affect self-renewal and pluripotency of human iPSCs, as pluripotency is conveyed via binding of an ARID1A-containing BAF to pluripotency-associated enhancers of the SOX2 and NANOG networks. On the other hand, we show that ARID1B-BAF is required for lineage specification and exit from pluripotency. In fact, ARID1B-BAF is only transiently active during early stages of iPSC-to-CNCC differentiation, and specifically during the formation of the neuroectodermal spheres, where it replaces ARID1A-BAF at the SOX2/NANOG enhancers and elicits their repression.
Importantly, we demonstrate that *ARID1B*$^{+/-}$ cells from Coffin-Siris patients are unable to switch from ARID1A-BAF to ARID1B-BAF at the onset of neuroectoderm formation, and instead maintain ARID1A-BAF at pluripotency enhancers throughout the entire differentiation process. Failure to replace ARID1A with

ARID1B leads to defective exit from pluripotency and impaired cranial neural crest formation. These findings provide evidence for a direct connection between *ARID1B* mutations and a pathogenic mechanism for ARID1B-associated neurodevelopmental syndromes.

## Results

### Coffin-Siris patient-derived iPSCs are pluripotent and proliferate normally

To investigate the function of ARID1B in craniofacial development, we obtained skin fibroblasts from two unrelated *ARID1B*$^{+/-}$ Coffin-Siris Syndrome patients (hereafter Patient-19 and Patient-26; Fig. 1a,b), one male and one female, both carrying previously identified *de novo ARID1B* mutations. In detail, Patient-19 presented a nonsense mutation (c.3223C>T;p.Arg1075*; Fig. 1b), while Patient-26 had a frameshift mutation (c.2598del;Tyr867Thrfs*47; Fig. 1b) [10,14]. In both cases, a premature STOP codon was generated (Fig. 1b).

The fibroblasts were reprogrammed into iPSCs by the LUMC hiPSC Hotel (Leiden University). Patient-derived iPSCs exhibited regular morphology (Fig. 1c) and expressed pluripotency genes, as shown by both immunofluorescence (Fig. 1d) and RT-qPCR (Fig. 1e). Further, patient-derived iPSCs grew at the same rate as an *ARID1B*$^{+/+}$ control line (Control line-1; Fig. 1f).

Importantly, the aberrant STOP codon introduced by the mutations was located either upstream (Patient-26) or inside (Patient-19) the AT-Rich Interactive Domain (ARID) (Fig. 1b), which is required for ARID1B's interaction with chromatin[22]. Moreover, in both patients, the new STOP codon was localized upstream of the Nuclear Localization Signal (NLS, Fig. 1b), suggesting that the gene product arising from the mutated allele would not be able to reach the nucleus or access the chromatin, even in the unlikely case that the transcript escaped non-sense mediated mRNA decay[23]. To test this, we performed cellular fractionation in patient and control iPSCs and conducted an ARID1B western blot on the chromatin fraction with an antibody raised against a peptide in the N-terminus of ARID1B, upstream of the mutated regions (sc-32762). Consistent with our hypothesis, the immunoblot on the chromatin fraction revealed a significantly reduced amount of ARID1B protein in both patient samples relative to the control *ARID1B*$^{+/+}$ iPSC line (Control line-1; Supplementary Figure S1a). ARID1B was reduced by approximately 60% and 80% in Patients 19 and 26, respectively. ARID1B was not detected in the cytoplasmic or nuclear fraction of any cell lines (Supplementary Fig S1a). Thus, *ARID1B* haploinsufficient iPSCs remained pluripotent, did not exhibit any growth defects, but did display significantly less chromatin-bound ARID1B than control iPSCs.

### CNCC formation is impaired in Coffin-Siris patient-derived iPSCs

Utilizing published methods for iPSC-to-CNCC differentiation[24] we generated CNCCs from control iPSCs, in 14 days (Fig. 2a,b). A time-course western blot conducted during the differentiation of Control line-1 revealed that ARID1B protein was robustly expressed during the first week of differentiation, peaking between days 5 and 7, with some expected variability between biological replicates (Fig. 2c; see Fig. 7 for a second replicate). After day 7; however, ARID1B protein was markedly downregulated (Fig. 2c). The window of robust ARID1B expression (day-1 to day-7) coincided with the differentiation of the iPSCs into neuroectodermal spheres, suggesting that this BAF subunit may have a role in neuroectoderm specification.

Next, we induced CNCC differentiation in two Coffin-Siris patient lines and compared them to Control iPSC-derived CNCCs using flow cytometry to measure multiple pluripotency (SSEA-4, TRA-1-60-R) and CNCC (CD10, CD99) surface markers. Cells were sampled at day-zero (iPSCs), day-5 (neuroectoderm), and day-14 (CNCC). Notably, CNCC formation was impaired in both patient-derived lines, as evident by a sizable cell population that was double-positive for pluripotency surface markers even after 14 days of differentiation (Fig. 2d; Supplementary Fig. S2). This double positive population comprised 4.5% and

146 19.5% of the cells in the two patient lines, respectively (Fig. 2d). In line with this, a large fraction of patient
147 cells showed significantly lower expression of CNCC surface markers even after 14 days of differentiation
148 relative to the control line (Fig. 2e).
149 To further characterize patient-derived CNCCs, we performed immunofluorescence for pluripotency
150 (OCT4, NANOG) and neural crest (SOX9) markers, in control and patient lines at day-14. Interestingly,
151 CNCCs derived from patient iPSCs displayed a gene expression signature distinct from that of control
152 CNCCs (Fig. 3). In fact, nearly all patient derived CNCCs were positive for SOX9, NANOG (Patients 19 and
153 26) and OCT4 (Patient 26 only; Fig. 3). This was in stark contrast to the control line, in which SOX9-positive
154 cells were almost all OCT4- and NANOG-negative (Fig. 3; See Supplementary Fig. S3 for quantifications
155 and p-values). Together, these data suggested that while *ARID1B* is dispensable for pluripotency,
156 haploinsufficiency of this gene severely impaired CNCC formation, resulting in CNCCs expressing key
157 pluripotency genes.
158
159 **Chromatin accessibility is dysregulated in differentiating Coffin-Siris patient-derived lines**
160 We used Next-Generation Sequencing to investigate why *ARID1B* haploinsufficient Coffin-Siris iPSCs did
161 not successfully differentiate into CNCCs. Given that ARID1B protein levels in control cells reach a peak
162 between days 5 and 7, samples were taken at day-5 to perform genomic analyses. Experiments were
163 conducted with two biological replicates per condition (two control lines, two patient lines). For each
164 condition, a male and a female were included to avoid sex-specific confounding effects. Technical
165 replicates were also used for each biological replicate. To avoid batch effects, all the biological replicates
166 and conditions were processed together.
167 Since ARID1B is a component of the BAF chromatin-remodeling complex, we profiled chromatin
168 accessibility with ATAC-seq. Overall, at day 5, 29,758 ATAC-seq peaks were identified across all replicates
169 and conditions (patients and controls; FDR <0.05; Fig. 4a). Conversely, 5,540 peaks were specific to the
170 patient iPSCs (i.e. replicated in all patient's iPSC replicates and not detected in any of the controls;
171 hereafter patient-specific ATAC-seq regions; Fig. 4a,b; Supplementary File S1). Finally, only 578 peaks
172 were specific to the controls (hereafter control-specific ATAC-seq regions; Fig. 4a,c; Supplementary File
173 S1). We therefore focused on the 5,540 patient-specific ATAC-seq regions because they represented 91%
174 (5,540/6,118) of all regions with differential chromatin accessibility between patient and control lines.
175 At day 0, ATAC-seq performed in iPSCs revealed that the 5,540 regions were highly accessible, with no
176 significant differences between patient and control lines (Supplementary Fig. S4a). By day 5, this
177 dramatically shifted and 5,511 of the 5,540 regions (99.4%) were called as peaks exclusive to the patient
178 lines. These data suggested that these were regions highly accessible in iPSCs and repressed by day 5 of
179 iPSC-to-CNCC differentiation. Such repression is impaired by *ARID1B*-haploinsufficiency, indicating that
180 chromatin accessibility in the 5,540 genomic sites may be directly regulated by an ARID1B-containing BAF
181 during exit from pluripotency and neuroectoderm specification. Thus, we investigated ARID1B's binding
182 at these regions both in day 0 (iPSCs) and in day 5 cells. At day 0, these regions were not bound by ARID1B
183 (Supplementary Fig. S4b). This was expected, given that that ARID1B is not a component of any of the BAF
184 configurations predominant in iPSCs and ESCs (esBAF and gBAF[4-6]), and likely explains why differences in
185 chromatin accessibility at these regions between patient and control lines at day 0 was not observed.
186 On the other hand, at the day 5, the 5,540 regions were bound by ARID1B in both control lines, while the
187 binding was almost entirely lost in both patient lines (Fig. 4d). This loss of binding correlated with lack of
188 chromatin repression in both patient lines. Together, these findings indicated that gain of ARID1B binding
189 at these 5,540 genomic sites in early stages of iPSC-to-CNCC differentiation may be required for repression
190 of the pluripotency program.
191
192 **The ARID1B-BAF attenuates thousands of enhancers at the onset of CNCC differentiation**

193 To determine the nature of the 5,540 genomic regions, we associated a gene to each region based on the
194 distance from the nearest Transcription Start Site (TSS). Overall, 87.5% of the ARID1B ChIP-seq peaks were
195 located >10 Kbs from the nearest TSS and may represent putative enhancers, while the remaining 12.5%
196 are likely promoters. ChIP-seq time-course for H3K27ac in control cells revealed that many of these
197 regulatory regions were enriched for H3K27ac in iPSCs, progressively lost this enrichment during
198 differentiation, and by day 5 had very reduced H3K27ac signal (Fig. 4e). The gradual decrease in H3K27ac
199 mirrored the steady increase in ARID1B expression detected during the early stages of iPSC-to-CNCC
200 differentiation, and specifically during the formation of the neuroectodermal spheres (Fig. 2c). Consistent
201 with this, the differentiating cells from both patients had significantly higher levels of H3K27ac in these
202 regions, relative to the two control lines at day 5 (Wilcoxon's Rank Sum Test $p < 2.2 \times 10^{-16}$ in all the patient
203 vs control pairwise comparisons; Fig. 4f, g).
204 We further investigated the fate of these regions over the course of iPSC-to-CNCC differentiation. We
205 found that while these cis-regulatory elements were still largely active in both patient lines at the day-7,
206 they were inactive in the control line (Fig. 4g). Interestingly, at day 9 of differentiation, these regions were
207 inactivated (i.e., no H3K27ac signal) in Patient-19 line, while remained active (i.e., persistent H3K27ac
208 signal) in the Patient-26 line (Fig. 4g).
209 Based on the high H3K27ac signal that the 5,540 patient-specific regions display at the iPSC stage (Fig. 4e),
210 we surmised that these sites could represent cis-regulatory elements important for pluripotency. In line
211 with this hypothesis, DNA-motif analysis on the 5,540 regions revealed that they were enriched for the
212 binding sites of multiple pluripotency factors, including SOX2 and NANOG (Fig. 4h; Supplementary File S2).
213 To ensure that the molecular phenotypes observed were directly caused by the *ARID1B* mutations, and
214 not by co-occurring mutations in other genes coincidentally shared by both (unrelated) patients we
215 employed shRNAs to knock-down ARID1B in the Control Line-1. We were able to obtain a partial knock-
216 down of ARID1B at the iPSC stage (shRNA-1; Supplementary Fig. 4c), which represented a suitable model
217 for *ARID1B* haploinsufficiency. ARID1B-KD iPSCs were put through the CNCC differentiation protocol and
218 collected at day 5, and profiled via ATAC-seq and ChIP-seq for H3K27ac. Notably, both sequencing
219 experiments perfectly recapitulated our findings in the patient-derived lines. Upon ARID1B-KD, we
220 detected significantly increased chromatin accessibility and H3K27ac signal in the 5,540 patients-specific
221 regions relative to the same iPSC line transduced with a control shRNA (Wilcoxon's Rank Sum Test $p < 2.2$
222 $\times 10^{-16}$; Supplementary Fig. S4d, e).
223 Together, these data indicate that ARID1B-BAF modulates the chromatin accessibility of a specific set of
224 ~4,900 pluripotency enhancers and ~600 promoters that are highly active in iPSCs, moderately active at
225 the onset of neuroectoderm formation, and inactive by day 7 and for the remaining course of CNCC
226 formation (Fig. 4e). These data suggested that impaired attenuation of these cis-regulatory elements in
227 the *ARID1B* haploinsufficient cells, subsequently hampers the entire differentiation process towards a
228 CNCC fate.
229
230 **<u>"Pluripotency" and "Exit from Pluripotency" genes are dysregulated in differentiating patient lines</u>**
231 Impaired attenuation of ~4,900 pluripotency-relevant enhancers and ~600 promoters could have a
232 profound effect on gene expression levels. Indeed, RNA-seq conducted at day 5 identified 2,356
233 differentially expressed genes, 1,685 of which were downregulated, and 671 upregulated (FDR <5%; 5a).
234 As expected, *ARID1B* was one of the top downregulated genes in patient CNCCs (Fig. 5a). In stark contrast,
235 only 54 genes were identified as differentially expressed when we performed RNA-seq at the iPSC stage
236 (FDR <5%). This suggested that ARID1B is important for lineage commitment, again mirroring the
237 progressive increase in the ARID1B protein level observed during early stages of differentiation (Fig. 2c).
238 The small number of differentially expressed genes identified at the iPSC stage was again consistent with
239 the finding that esBAF and gBAF do not include ARID1B[4-6].

240 Notably, 598/2,356 (25.4%) of the genes differentially expressed at day 5 also represented the nearest
241 gene to one of the 5,540 pluripotency enhancers and promoters aberrantly active in the Coffin-Siris
242 patient cells at the same time point (Supplementary File S3). These results suggested that over a quarter
243 of differentially expressed genes were under the direct control of ARID1B-BAF throughout modulation of
244 chromatin accessibility at associated enhancers and promoters. As expected, when we compared these
245 598 genes against the entire set of 2,356 differentially expressed genes, we found that the 598 genes
246 exhibited enrichment for genes upregulated in patient cells (Fisher's Exact Test $p < 0.0001$). Ingenuity
247 Pathway Analysis on the 598 genes identified five of the top canonical pathways as associated with either
248 pluripotency or exit from pluripotency, as well as Wnt-β catenin signaling pathway[25,26] (Fig. 5b;
249 Supplementary File S4).
250 In accordance with the ATAC-seq data, SOX2 was detected among the top upstream regulators (Fig. 5c),
251 and three of the most important pluripotency factors, *NANOG, SOX2* and *POU5F1* (OCT4), were highly
252 expressed in the patient lines at day 5 (Fig. 5d).
253 Both the "*Role of NANOG in Mammalian Embryonic Stem Cell Pluripotency"* and the "*PPARα/RXRα*
254 *Activation"* pathways were enriched in the 598 genes (Fig. 5b). Namely, the genes belonging to the former
255 pathway were all upregulated, while those belonging to the latter were downregulated (Fig. 5d). These
256 two pathways caught our attention because they are thought to antagonize each other. More specifically,
257 NANOG blocks the differentiation of pluripotent cells and establishes the pluripotent state during somatic
258 cell reprogramming. Conversely, the PPARα/RXRα pathway is activated at the onset of differentiation to
259 promote exit from pluripotency[27]. The activation of PPARα/RXRα contributes to the repression of the
260 *NANOG* network to allow efficient exit from the undifferentiated stage[27-29]. Consistent with this, PPARα-
261 inhibitors have been employed to improve iPSC reprogramming[27].
262 These gene expression data were in agreement with the immunofluorescence findings and with the
263 perpetual *NANOG* and *OCT4* expression in patient derived CNCCs at day 14 of differentiation (Fig. 3).
264 Finally, we looked for potential overlap between our set of 2,356 differentially expressed genes at day 5
265 of iPSC differentiation toward CNCC and a set of genes identified as differentially expressed in a recent
266 RNA-seq study which compared cerebellar tissue of *ARID1B*$^{+/-}$ and *ARID1B-wt* mice[30]. Notably, 1,297 of
267 the 2,356 genes (55%) found as differentially expressed in our study were also found as differentially
268 expressed in the KO-mouse model dataset. This overlap (55%) was significantly higher than expected by
269 chance (Fisher's Exact Test $p < 2.2 \times 10^{-16}$) and suggested that the pathways regulated by ARID1B are
270 important for both craniofacial and brain development.
271 Taken together, our RNA-seq data suggested that differentiating *ARID1B*$^{+/-}$ patient-derived lines exhibited
272 a persistent upregulation of multiple pluripotency factors and associated gene networks, along with
273 downregulation of genes responsible for exit from pluripotency. Dysregulation of these gene networks
274 subsequently impaired neuroectoderm specification and CNCC formation.
275
276 **Aberrant SOX2 and NANOG activity in the *ARID1B* haploinsufficient patient cells**
277 Our experiments indicate that the *ARID1B* haploinsufficient cells fail to attenuate thousands of
278 pluripotency enhancers and promoters enriched for SOX2 and NANOG binding sites (Fig. 4a–h). Further,
279 at day-5 of iPSC-to-CNCC differentiation, the expression of *SOX2* and *NANOG* is significantly higher in the
280 patient derived cells than in the controls, and the gene regulatory networks associated with these
281 pluripotency factors are also upregulated (Fig. 5b–d). Moreover, both patient-derived CNCCs (day-14)
282 exhibit aberrant expression of NANOG (Fig. 3).
283 Given these findings, we set out to investigate the binding profile of SOX2 and NANOG in patient and
284 control lines by ChIP-seq at CNCC day-5. Our spike-in normalized SOX2 ChIP-seq revealed that 3,284/5,540
285 (59.7%) patient-specific ATAC-seq peaks exhibit significantly higher SOX2 binding in patients relative to
286 control lines (Fig. 6a). In line with this, the chromatin at these regions is accessible in the patient lines but
287 not in the control lines (Fig. 6b). SOX2 is a pioneer factor that can bind condensed nucleosomes to open

288 the chromatin and allow binding of other factors[31]. As demonstrated by previous studies in mouse
289 embryonic stem cells (mESCs), SOX2 and other pluripotency pioneer factors (e.g. OCT4) require the BAF
290 complex to perform their pioneer activity[6,31,32]. Our findings indicate that, in control conditions, the
291 ARID1B-BAF complex likely antagonizes the cooperation between other BAF configurations and SOX2,
292 counter-acting the pioneer activity of the latter as soon as cell differentiation is induced. Further, we
293 identified an additional set of 497 SOX2 peaks specific to the patient lines, which did not exhibit changes
294 in chromatin accessibility. Moreover, we also identified 1,146 SOX2 peaks exclusive of the control lines
295 (Supplementary File S5). Importantly, these control-specific SOX2 peaks were located in proximity to
296 genes associated with neural crest differentiation, including *TFAP2A*, *PAX6*, *PAX7*, *WNT4*, *ENO1*, *C8B*, and
297 *SERBP1* among others. These findings are consistent with two recent studies which suggested that SOX2-
298 chromatin interactions are rewired upon differentiation cues[33,34]. Such rewiring appears impaired in
299 *ARID1B*-haploinsufficient cells, which aberrantly maintain SOX2 at pluripotency-associated enhancers,
300 and at the same time fail to reposition this transcription factor at the developmental enhancers.
301 Next, we profiled NANOG at day-5 of differentiation. For this transcription factor, the spike-in normalized
302 ChIP-seq revealed 4,538 peaks unique to the patients (Supplementary File S6). However, in this case, only
303 219 (4.8%) of the patient-specific NANOG peaks overlapped a patient-specific ATAC-seq peak. We thus
304 interrogated our ATAC-seq data to determine the state of chromatin accessibility at the 4,538 patient-
305 specific NANOG peaks, and overall found no significant changes in accessibility in these regions between
306 the patients and the control lines (Fig. 5c). We note that nearly a quarter of the patient-specific NANOG
307 peaks were found in regions of repressed chromatin (Fig. 6c,e), in line with recent studies which suggested
308 that NANOG can bind repressed chromatin like other pioneer pluripotency factors[35,36].
309 Despite no changes in chromatin accessibility, the NANOG ChIP-seq signal at the 4,538 patient-specific
310 NANOG peaks was significantly higher in the patient than in the control lines (Wilcoxon's Rank Sum Test
311 $p < 2.2 \times 10^{-16}$ in all the patient vs control pairwise comparisons; Fig. 6d,e). We hypothesized that the
312 increased NANOG binding detected in the patients' cells (Fig. 6d) could reflect increased *NANOG*
313 expression (Fig. 6d). In fact, several elegant studies in embryonic stem cells have demonstrated that
314 changes in *NANOG* dosage mark the transition from an undifferentiated state (high *NANOG*), to a state
315 with differentiation potential (low *NANOG*)[37-39]. Importantly, it has been shown that SOX2 and OCT4 bind
316 a cis-regulatory element in the promoter region of *NANOG*, likely modulating its expression[40,41]. Thus, we
317 examined this cis-regulatory element in detail. As expected, at day-5 of iPSC-to-CNCC differentiation, the
318 chromatin accessibility at the promoter-proximal element is significantly higher in the two patient lines
319 than in the two controls (Student's T-Test $p$=0.0065; Fig. 6f). Accordingly, increased chromatin
320 accessibility correlates with increased SOX2 binding on the cis-regulatory element (Fig. 6f), perhaps
321 explaining the higher *NANOG* gene expression reported in patient-derived lines at day-5. Lastly, our
322 shRNA experiments also confirmed these findings, demonstrating that the knock-down of ARID1B in the
323 Control line-1 line correlates with a sizeable increase in accessibility at the *NANOG* cis-regulatory element
324 (Fig. 6g), thus suggesting that ARID1B-BAF directly modulates *NANOG* expression dosage at the onset of
325 differentiation.
326 In sum, the *ARID1B* haploinsufficient lines exhibit persistent activity of two key pluripotency factors (SOX2,
327 NANOG) in the early and late stages of CNCC formation. The aberrant activity of SOX2 and NANOG likely
328 leads to impaired lineage commitment and inefficient CNCC formation.
329
330 **A switch from ARID1A-BAF to ARID1B-BAF is necessary for exit from pluripotency**
331 We next wanted to elucidate how the BAF complex compensated for *ARID1B* haploinsufficiency. As
332 mentioned above, ARID1A and ARID1B represent the only two subunits of the BAF harboring an ARID
333 domain, which is leveraged by the complex to interact with the chromatin[22]. A third ARID subunit (ARID2)
334 is exclusive to a different configuration of the complex (pBAF). *ARID2* mutations have been shown to cause
335 a neurodevelopmental disorder that does not fully recapitulate the Coffin-Siris syndrome phenotype,

336 although there is some overlap[42]. Compensatory mechanisms between ARID1A and ARID1B were recently
337 demonstrated in ovarian cancer[43]. Thus, we hypothesized that *ARID1B* haploinsufficient patient-derived
338 cells may compensate for partial loss of ARID1B with ARID1A. To test this, we first assessed ARID1A protein
339 levels in *ARID1B*-wt cells during CNCC formation and found that ARID1A expression was complementary
340 to ARID1B (Fig. 7a). In agreement with the specific composition of the esBAF, which requires ARID1A[5,6],
341 human iPSCs expressed high levels of ARID1A and relatively low ARID1B (Fig. 7a). On the other hand, at
342 the initiation of iPSC-to-CNCC differentiation (day 1) ARID1B was upregulated while ARID1A was strongly
343 repressed to levels barely detectable (Fig. 7a). ARID1B remained the only active ARID1 subunit between
344 days 1-5 (i.e., during the formation of the neuroectodermal cells; Fig. 7a). Finally, at day 7, ARID1B was
345 abruptly downregulated and ARID1A was restored at high levels at day 9. This latter switch corresponded
346 to the beginning of the differentiation of the neuroectodermal spheres into migratory CNCCs (Fig. 7a).
347 Together, these data suggested that throughout the course of CNCC differentiation, multiple switches
348 between ARID1A and ARID1B occur, and that these two ARID1 subunits regulate specific developmental
349 stages during CNCC formation.
350 Next, we profiled ARID1A protein levels during iPSC-to-CNCC differentiation in patient derived lines. Time-
351 course immunoblotting revealed that the temporary decommissioning of ARID1A during neuroectoderm
352 specification (~days 1-7) failed to occur in both of the patient cell lines (Fig. 7b). In fact, in the patient
353 lines, ARID1A protein levels were maintained throughout the course of iPSC differentiation (days 1-11)
354 (Fig. 7b).
355 In addition to perpetual expression, there was an approximate 5-fold increase in ARID1A expression in
356 patient cell lines, relative to controls at day 5 (Patient 19: 4.9-fold; Patient 26: 5.1-fold; Fig. 7c), a time
357 point which exhibited robust ARID1B expression in control cells. Together, these data suggested that the
358 patient cells compensated for the partial loss of ARID1B by maintaining aberrantly high ARID1A levels
359 throughout the differentiation process.
360 A recent study conducted on liver cells demonstrated that ARID1A- and ARID1B-containing BAF may have
361 antagonistic functions in the transcriptional regulation of specific genes, with ARID1B acting prevalently
362 as a repressor of enhancer elements, as opposed to the ARID1A, which mostly functions as an activator[44].
363 Hence, we hypothesized that the perpetual and robust ARID1A protein levels detected in patient-derived
364 cells during iPSC-to-CNCC differentiation, and specifically during neuroectoderm specification, may result
365 in prolonged activity of pluripotency enhancers. Consistent with the recent studies which reported that
366 the (ARID1A-containing) esBAF regulates pluripotency genes in iPSCs and ESCs[4-6], ARID1A ChIP-seq
367 performed at the iPSC stage revealed that the 5,540 pluripotency enhancers and promoters were bound
368 by ARID1A in all the four lines (Fig. 7d). Conversely, the same experiment conducted at day 5 of
369 differentiation revealed that while ARID1A-binding was lost at the 5,540 pluripotency elements in control
370 cell lines, it was maintained in patient cell lines (Fig. 7d). In summary, these data indicated that the status
371 of a set of ~5,500 pluripotency enhancers and promoters was regulated by ARID1A at the iPSC stage and
372 by ARID1B during exit from pluripotency and neuroectodermal lineage commitment. Importantly,
373 *ARID1B*-haploinsufficiency in patient cell lines triggered a compensatory mechanism which resulted in
374 persistent binding of ARID1A at pluripotency enhancers throughout differentiation.
375
376 **The ARID1B-BAF complex exclusively incorporates SMARCA4 as an ATPase subunit**
377 Finally, we addressed the composition of the ARID1B-BAF complex at day 5 of iPSC-to-CNCC
378 differentiation. To do so, we performed immunoprecipitation of endogenous ARID1B followed by mass-
379 spectrometry (IP-MS). In control cells, ARID1B coeluted with a total of ten additional BAF subunits
380 (hereafter ARID1B-BAF; Supplementary Fig. S5a). In mammals, BAF complexes incorporate two widely
381 interchangeable and mutually exclusive ATPase subunits, SMARCA2, and SMARCA4. Remarkably,
382 SMARCA4 was the only ATPase subunit identified as coeluting with ARID1B in our IP-MS, while zero
383 peptides of SMARCA2 were detected (Supplementary Fig. S5a). This suggests that ARID1B-BAF selectively

384 incorporates only SMARCA4 as a catalytic subunit, while it does not tolerate the incorporation of
385 SMARCA2.
386 We repeated this experiment in the patient-lines to determine if perpetually active ARID1A replaced
387 ARID1B in the ARID1B-BAF or if instead it was part of a completely different BAF configuration. We thus
388 performed ARID1A IP-MS at day 5 in patient lines. Notably, in the two patient lines ARID1A co-eluted with
389 all the other subunits of the ARID1B-BAF (Supplementary Fig. S5b). In summary, the perpetual presence
390 of ARID1A-BAF in patient cells correlated with a very specific (and previously uncharacterized)
391 configuration of the BAF complex (ARID1B-BAF), which was active during exit from pluripotency and
392 neuroectoderm formation.
393 Intriguingly, the transcription factor SALL4 also coeluted with ARID1B at day 5, suggesting a possible
394 interaction with the complex. Like ARID1B, SALL4 is also dispensable for the maintenance of the
395 pluripotency networks, while it is essential for lineage commitment in early mammalian development,
396 during which it targets sites with binding motifs also recognized by SOX2, OCT4 and NANOG[45-48]. SALL4
397 was previously shown to interact with the NuRD repressive complex[46], while interactions with BAF have
398 been largely unexplored. It was recently demonstrated that this transcription factor has affinity for AT-
399 rich regions[49], thus providing further support to the ARID1B-SALL4 interaction. *SALL4* mutations are also
400 associated with developmental syndromes, including Okihiro syndrome, Holt-Oram syndrome, and
401 Townes-Brocks Syndrome[50]. Notably, the *SALL4* gene is downregulated in the Coffin-Siris patients at CNCC
402 day-5 but not in undifferentiated iPSCs, suggesting a possible feedback mechanism between *ARID1B* and
403 *SALL4* during lineage commitment. Future studies will be necessary to support the speculation that SALL4
404 serves as an intermediator for ARID1B-BAF recruitment at the pluripotency enhancers.
405
406 **Discussion**
407 ARID1B is a member of the evolutionarily conserved SWI/SNF (BAF) chromatin remodeler[22,51]. *De novo*
408 haploinsufficient mutations in the *ARID1B* gene cause severe neurodevelopmental disorders which affect
409 both physical and cognitive development. In this study, we investigated the role of Coffin-Siris-associated
410 *ARID1B* mutations in the context of craniofacial development and report the discovery of a novel function
411 of the BAF complex: attenuation of the gene expression program associated with pluripotency
412 maintenance upon differentiation cues. We found that this repressive function is performed at
413 pluripotency enhancers and promoters by a specific and novel BAF complex configuration (ARID1B-BAF),
414 which is composed of 9 subunits, with the enzymatic activity seemingly carried out exclusively by
415 SMARCA4.
416 As a consequence of the *ARID1B* mutations, Coffin-Siris patient cells fail to repress the pluripotency
417 elements. This subsequently elicits aberrant SOX2 activity genome-wide, which in turn leads to the
418 upregulation of multiple pluripotency genes, including *NANOG* and its associated gene network, and to
419 the downregulation of the genes responsible for coordinating the exit from pluripotency
420 (PPAR$\alpha$/RXR$\alpha$ pathway). We demonstrated that these pluripotency enhancers are normally maintained
421 in an active state by ARID1A-BAF at the iPSC stage, and subsequently repressed by the ARID1B-BAF
422 throughout neuroectoderm formation, which is the first stage of CNCC development.
423 A switch between ARID1A-BAF and ARID1B-BAF upon differentiation cues is hence necessary for
424 commitment towards the neuroectodermal lineage. We additionally report that a second switch from
425 ARID1B-BAF to ARID1A-BAF takes place later, when the neuroectodermal spheres differentiate into
426 CNCCs. This suggests that ARID1B is likely the dominant ARID1 subunit during neuroectoderm
427 specification, while ARID1A regulates the following stage, during which the neuroectodermal spheres
428 differentiate into migratory CNCCs. It is worth noting that the neuroectoderm not only gives rise to all
429 regions of the brain and central nervous system (hindbrain, midbrain, forebrain, spinal cord and motor
430 neurons), but also gives rise to the neural crest cells, which emanate out from the dorsal aspect of the
431 neural tube. Therefore, we speculate that the dysregulation of neuroectoderm specification caused by

432 *ARID1B* mutations may underlie both the cognitive impairment and craniofacial abnormalities that are
433 typical of Coffin-Siris syndrome. This model is further supported by a significant overlap of differentially
434 expressed genes identified in our study (neural crest formation) and in a recently published *ARID1B*-KO
435 mouse model (brain tissue)[30].
436 Other studies have previously suggested that switches between SWI/SNF subunits play important roles in
437 cell fate determination. For example, a switch between the two catalytic subunits SMARCA4 and
438 SMARCA2 mediates the activation of human IFNγ-activated genes[52]. Similarly, a gain of the subunit
439 BAF53a in the neuron-specific BAF (nBAF) is required to control cell cycle exit in developing neurons[2,3].
440 With our study, we discovered a novel, binary switch between BAF subunits (ARID1A/ARID1B), critical for
441 the exit from pluripotency. Importantly, a balance between pro-self-renewal and pro-differentiation
442 signals is pivotal for the determination of stem cell fate[53]. We demonstrate that such balance is lost in
443 Coffin-Siris patients, whose cells are unable to perform the ARID1A/ARID1B switch at the pluripotency
444 enhancers at the onset of differentiation. This switch is essential to successfully complete CNCC
445 differentiation.
446 Pluripotency is orchestrated by a transcription factor network that needs to be extinguished in an orderly
447 manner to enable lineage commitment and differentiation[53-55]. We find that ARID1B-BAF plays an
448 essential role in this process, by means of repressive activity at pluripotency enhancers for the SOX2,
449 NANOG, and OCT4 networks. Similarly, an association between SOX3 and the SMARCA2 ATPase subunit
450 of BAF was recently suggested in a study of neural development in the Nicolaides-Baraitser syndrome[56].
451 It is worth noting that Coffin-Siris and Nicolaides-Baraitser syndromes share many physical and
452 neurological phenotypes[56-58].
453 The BAF complex is predominantly considered as a transcriptional activator, which balances the Polycomb
454 Repressor Complexes (PRC1, PRC2) in the modulation of gene expression[7,59]. Despite this widely held
455 belief, repressive activity for BAF has been reported. For instance, a study conducted on hepatocellular
456 carcinoma cell lines uncovered that ARID1A-containing BAF activates and represses roughly equal
457 numbers of genes, while ARID1B-containing BAF was found to primarily repress enhancer activity[44]. Our
458 experiments corroborate these findings, supporting an enhancer-repressor function for ARID1B-BAF. We
459 demonstrate that the repressive activity of ARID1B-BAF is specific to a set of ~4,900 enhancers and ~600
460 promoters, enriched for SOX2 and NANOG binding sites. In control cells, these cis-regulatory elements are
461 highly active at the iPSC stage, moderately active in the first four days of differentiation, and finally
462 repressed by day 5, a time point at which we observed the peak of ARID1B protein expression. Coffin-Siris
463 patient-derived iPSC lines exhibit aberrant chromatin accessibility at these cis-regulatory elements for
464 many days after the onset of iPSC-to-CNCC differentiation, enforcing a perpetual pluripotency signature
465 which persists even after two weeks of differentiation.
466 Patient-26-derived cells display the most extreme cellular and molecular phenotype, with a large
467 population of cells remaining pluripotent at day-14 of differentiation, likely as a consequence of higher
468 *SOX2, OCT4* and *NANOG* expression and activity. Cells derived from this patient also show the highest
469 levels of ARID1A binding at these enhancers at day 5 of CNCC differentiation. Although it is difficult to
470 formally compare disease severity since there are no accepted severity scales for Coffin-Siris syndrome, it
471 is worth noting that Patient-26 had a more severe disease process than Patient-19. For example, Patient-
472 26 was not able to speak at 7 years, whilst Patient-19 started speaking at 4 years. Additionally, Patient-26
473 was affected by pyloric stenosis, a congenital anomaly in the digestive tract thought to be associated with
474 impaired migration of the enteric neural crest. We consider it unlikely that the difference is caused solely
475 by the mutations in *ARID1B*, since both patients show comparable reduction in ARID1B protein levels. We
476 speculate that additional genetic factors may cooperate with *ARID1B* haploinsufficiency to determine the
477 clinical severity of the syndrome. However, additional experiments with a larger set of patient-derived
478 cell lines would be required to support this model. Furthermore, it would also be important to investigate
479 other differentiation lineages to elucidate whether the ARID1A/ARID1B switch is only important for neural

480 crest differentiation or if, instead, it represents a more widespread mechanism utilized by stem cells to
481 exit the pluripotent state and undergo lineage commitment.
482 Finally, further investigations will be necessary to elucidate the mechanism(s) responsible for the
483 repressive activity of ARID1B-BAF. Recent studies have demonstrated that the function of BAF (including
484 ARID1A-BAF) as transcriptional activator is mediated by the AP-1 transcription factors[56,60,61]. On the other
485 hand, little is known of potential co-factors mediating the repressive function of ARID1B-BAF.
486
487 **Acknowledgements**
488 The authors are deeply grateful to the patients and their families, who donated the samples for this
489 research. The authors thank the physicians and technicians who collected and cultured the skin
490 samples. This work was funded by the G. Harold and Leila Y. Mathers Foundation (MT), and the Gisela
491 Thier Fellowship (GWES). The authors thank the Genomic Facilities at Thomas Jefferson University and at
492 the Wistar Institute for the sequencing effort. The authors are grateful to Kelly Vonk (Leiden University)
493 for the help with experimental procedures in the iPSC generation. An invaluable support was provided to
494 the authors by the Stem Cell and Regenerative Neuroscience Center at Thomas Jefferson University, and
495 in particular by Dr. Elizabeth Kropf. Lastly, MT and GWES are thankful to Dr. Samantha Vergano (Children's
496 Hospital of the King Daughters) for making this collaboration and this work possible.
497
498 **Author contributions**: MT, GWES and LP designed the project. GWES recruited the patients and obtained
499 the skin fibroblasts. HMMM and CF reprogrammed the patient fibroblasts into iPSCs and assessed their
500 quality. LD performed initial iPSC characterization experiments. LP performed most of the experiments,
501 with crucial contributions from PP. ATC, CS, CAO, and SAW contributed to specific experiments
502 (flowcytometry, immunoblots, mass-spectrometry). BC provided intellectual contribution and financial
503 support to PP. SAB provided helpful discussion and editing. MT, LP, PP and SD analyzed the data. MT,
504 GWES, PP, and LP wrote the manuscript, which was read and approved by all the authors.

505 **Data availability:** The original genome-wide data generate for this paper are deposited in the GEO
506 database (accession number GSE169654).

507 **Figure legends**
508
509 **Figure 1 – iPSCs derived from Coffin-Siris patients are pluripotent and proliferate normally. (a)** Study
510 system: iPSCs were derived from skin fibroblasts of two unrelated Coffin-Siris patients. The iPSCs were
511 used in this study to generate Cranial Neural Crest Cells (CNCCs) and perform genomic experiments to
512 investigate the effect of *ARID1B* mutations. **(b)** Graphical illustration of the *ARID1B* haploinsufficient
513 mutations affecting the two studied patients. The numbers in the gene model refer to *ARID1B's* isoform
514 NM_020732.3. **(c)** Colony of iPSCs derived from Patient-19 showing typical iPSC morphology. **(d, e)**
515 Immunofluorescence and rt-qPCR quantifying the expression of the key pluripotency markers in iPSCs
516 derived from Control and Patient lines. P-values are from Student's T-test (* = $p < 0.05$; ** $p < 0.005$; ***
517 = $p < 0.0005$). **(f)** Growth curve comparing an *ARID1B*-wt Control iPSC Line with the two patient lines. The
518 patient cells do not exhibit growth impairment. P-values are from Student's T-test (* = $p < 0.05$; ** $p <$
519 $0.005$; *** = $p < 0.0005$).
520
521 **Figure 2 – CNCC differentiation is impaired in the patient cells. (a, b)** CNCC differentiation was optimized
522 using an *ARID1B*-wt Control Line. After 14 days, the cells exhibited the classic CNCC morphology and
523 expressed the CNCC markers. P-values are from Student's T-test (* = $p < 0.05$; ** $p < 0.005$; *** = $p <$
524 $0.0005$). **(c)** Time-course immunoblot conducted using Control Line-1 during CNCC differentiation shows
525 that ARID1B is active in the first 7 days of the differentiation, with a peak of activity between day-5 and

526 day-7. The ARID1B protein level strongly decreases after day-7. **(d, e)** Flowcytometry quantifying
527 expression of surface markers for pluripotency and CNCC differentiation in control line-1 and in the two
528 patient lines. A large cell population is still pluripotent in both patients after 14 days (d). The patient lines
529 also show reduced expression of CNCC surface markers after 14 days of differentiation relative to an
530 *ARID1B*-wt Control Line at the same time point (e).
531
532 **Figure 3 – Aberrant NANOG and OCT4 activity in the patient-derived CNCC**. Immunofluorescence for
533 SOX9, NANOG, and OCT4 performed at the day-14 of iPSC-to-CNCC differentiation in Control Line-1,
534 Patient-19 and Patient-26 cells. The patient cells are aberrantly NANOG-positive, and Patient-26 is also
535 OCT4-positive.
536
537 **Figure 4** – **Chromatin remodeling at pluripotency enhancers is dysregulated in the patient cells. (a)** At
538 CNCC day-5, 29,578 ATAC-seq peaks are shared between patient and control lines. 5,540 peaks are specific
539 of the patients. 578 peaks are specific of the controls. **(b)** UCSC Genome Browser example of a PATIENT-
540 SPECIFIC ATAC-seq peak. **(c)** UCSC Genome Browser example of a CONTROL-SPECIFIC ATAC-seq peak. **(d)**
541 ARID1B ChIP-seq heatmaps (Four lines; CNCC Day-5) centered on the PATIENT-SPECIFIC ATAC-seq peaks
542 **(e)** Heatmaps of H3K27ac ChIP-seq time-course at the 5,540 PATIENT-SPECIFIC ATAC-seq peaks (Control
543 Line-1). **(f)** H3K27ac ChIP-seq average profiles centered on the PATIENT-SPECIFIC ATAC-seq regions (CNCC
544 Day-5). Statistical significance assessed with Wilcoxon's Rank Sum test ($p < 2.2 \times 10^{-16}$ in all the patient vs
545 control comparisons). **(g)** Heatmaps of H3K27ac ChIP-seq signal at Days 5, 7, and 9 at the 5,540 PATIENT-
546 SPECIFIC ATAC-seq peaks (Control Line-1, Patient-19, Patient-26). **(h)** Motif analysis at the PATIENT-
547 SPECIFIC ATAC-seq regions revealed enrichment for the binding motif of multiple pluripotency factors.
548
549 **Figure 5** – "**Pluripotency" and "Exit from Pluripotency" genes are dysregulated in differentiating patient**
550 **CNCCs. (a)** RNA-seq volcano plot shows the differentially expressed genes between patient and control
551 lines at CNCC Day-5. *ARID1B* is one of the top downregulated genes. **(b)** Top canonical pathways (IPA
552 analysis) enriched in the set of 598 differentially expressed genes that also represent the closest gene to
553 a PATIENT-SPECIFIC ATAC-seq peak. **(c)** Top upstream regulators (IPA analysis) enriched in the same set
554 of 598 genes used for panel b. **(d)** RNA-seq heatmap displaying expression patterns at CNCC Day-5 for
555 pluripotency genes, for genes of the NANOG network, and for genes associated to exit from pluripotency
556 (PPARα/RXRα activation pathway).
557
558 **Figure 6 – Aberrant SOX2 and NANOG activity in the patient cells at CNCC Day-5. (a)** SOX2 ChIP-seq
559 average profile for 3,284 patient-specific ATAC-seq peaks showing patient-specific SOX2 signal (spike-in
560 normalized; CNCC Day-5). Statistical significance assessed with Wilcoxon's Rank Sum test ($p < 2.2 \times 10^{-16}$ in
561 all the patient vs control comparisons). **(b)** ATAC-seq heatmaps at the 3,284 peaks shown in Fig. 5a reveal
562 that these regions display increased chromatin accessibility in the patients relative to the two control
563 lines. **(c)** ATAC-seq heatmaps at 4,538 patient-specific NANOG peaks display no changes in accessibility
564 between patient and control lines. **(d)** NANOG ChIP-seq heatmaps at 4,538 patient-specific NANOG peaks
565 (spike-in normalized; CNCC Day-5). **(e)** Example of patient-specific NANOG peak in a region with no
566 chromatin accessibility (CNCC Day-5). **(f)** At CNCC Day-5, a cis-regulatory element in the promoter region
567 of *NANOG* is more accessible in the patients than in the control lines. The same element also displays
568 higher SOX2 binding in the patients than in the controls. **(g)** Knock-down of ARID1B from Control Line-1
569 also elicits an increase in chromatin accessibility at the cis-regulatory element in the promoter region of
570 *NANOG* (CNCC Day-5).
571
572 **Figure 7 – A switch between ARID1A-BAF and ARID1B-BAF is required for a successful exit from**
573 **pluripotency. (a)** Time-course immunoblot conducted using Control Line-1 during CNCC differentiation

shows that ARID1A is active at the iPSC stage, and abruptly downregulated at day-1 of differentiation. ARID1A protein level is upregulated again after day-7, mirroring ARID1B's downregulation at the same time point. **(b)** ARID1A time-course immunoblot in the two patient lines. **(c)** ARID1A immunoblot: both patient lines display aberrantly high ARID1A's protein level at CNCC Day-5. **(d)** ChIP-seq for ARID1A in the two control lines and the two patient lines at iPSC stage (day-0) and at CNCC Day-5. Heatmaps are centered on the 5,540 pluripotency enhancers.

## MATERIALS AND METHODS

### Human iPSC culture

Control iPSC lines were obtained from the iPSC Core of the University of Pennsylvania (Control line-1: SV20 line, male, age 43) and from the Coriell Institute for Medical Research (Camden, NJ. Control line-2: GM23716, female, age 16).

Skin fibroblasts from the two pediatric Coffin-Siris patients (one teenager one young adult) were obtained by the team of Dr. Gijs Santen at Leiden University. Patient 19 is a female, while Patient 26 is a male. The fibroblasts were reprogrammed into iPSCs with the polycistronic lentiviral vector LV.RRL.PPT.SF.hOKSM.idTomato.-preFRT by LUMC human iPSC Hotel as described elsewhere[62,63].

Multiple clones per line were derived. For each clone, pluripotency was assessed by immunofluorescence microscopy using antibodies against NANOG, OCT3/4, SSEA4 and Tra-1-81 under maintenance conditions and antibodies against (TUBB3, AFP and CD31) after spontaneous differentiation into the 3 germ layers as described elsewhere[62]. Clones with proper pluripotent characteristics were selected for downstream usage. Karyotyping by G binding was assessed for all the four lines by the Leiden University Medical Center and Short Tandem Repeat (STR) profiling was performed by the Leiden University Medical Center and and then replicated by the Stem Cell and Regenerative Neuroscience Center at Thomas Jefferson University. The iPSC lines were expanded in feeder-free, serum-free mTeSR™1 medium (STEMCELL Technologies). Cells were passaged ~1:10 at 80% confluency using ReLeSR (STEMCELL Technologies) and small cell clusters (50–200 cells) were subsequently plated on tissue culture dishes coated overnight with Geltrex™ LDEV-Free hESC-qualified Reduced Growth Factor Basement Membrane Matrix (Fisher-Scientific).

### CNCC Differentiation

The iPSC lines were differentiated into CNCC as previously described[24]. Briefly, iPSCs were treated with CNCC Derivation media: 1:1 Neurobasal medium/D-MEM F-12 medium (Invitrogen), 0.5× B-27 supplement with Vitamin A (50× stock, Invitrogen), 0.5× N-2 supplement (100× stock, Invitrogen), 20 ng/ml bFGF (Biolegend), 20 ng/ml EGF (Sigma-Aldrich), 5 µg/ml bovine insulin (Sigma-Aldrich) and 1× Glutamax-I supplement (100× stock, Invitrogen). Medium (3ml) was changed every day. Three days after the appearance of the migratory CNCC, cells were detached using accutase and placed into geltrex-coated plates. The early migratory CNCCs were then transitioned to CNCC early maintenance media: 1:1 Neurobasal medium/D-MEM F-12 medium (Invitrogen), 0.5× B-27 supplement with Vitamin A (50× stock, Invitrogen), 0.5× N-2 supplement (100× stock, Invitrogen), 20 ng/ml bFGF (Biolegend), 20 ng/ml EGF (Sigma-Aldrich), 1 mg/ml bovine serum albumin, serum replacement grade (Gemini Bio-Products # 700-104P) and 1× Glutamax-I supplement (100× stock, Invitrogen).

### ARID1B Knock-down

To make concentrated lentivirus, HEK293T cells were transfected with a pLenti plasmid in which we cloned an shRNA for *ARID1B* (GPP Web Portal: TRCN0000107361). iPSCs were lentivirally transduced by incubating the cells with concentrated virus overnight at 37 C. The next morning the media was changed, and 2 mg/ml puromycin (InvivoGen) were added 24h after infection. After 72 hours, the iPSCs that

survived the selection were then differentiated in CNCC using the above described protocol, and collected at Day-5 for the genomic experiments. The cells were kept under puromycin selection for the entire duration of the differentiation. The knock-down efficiency was quantified via western blot.

**Flow cytometry analysis of surface markers**

To obtain a single cell suspension for flow cytometry analysis, control and patient cells were treated with Accutase for 5 minutes. Cells were then washed with cold PBS-2% FBS and live cells were counted. $1 \times 10^6$ cells/condition were resuspended in 100 μL PBS-2% FBS and stained. For pluripotency evaluation, 4 µl of the respective antibodies were used: APC anti-human SSEA-4 antibody (Biolegend, #330417) and PE anti-human TRA-1-60-R antibody (Biolegend, #330609). For analysis of differentiation, 2 µl of the respective antibodies were used: FITC anti-human CD10 (Miltenyi Biotec, #130-124-262) and APC anti-human CD99 (Miltenyi Biotec, #130-121-096). Cells were incubated for 15 min on ice and protected from light, before transferring them into FACS tubes containing additional 300 μL PBS-2% FBS. Flow cytometry data were acquired using a BD LSR II flow cytometer and analyzed with FlowJo Software version 10.7.

**Western Blot**

For total lysate, cells were harvested and washed three times in 1X PBS and lysed in RIPA buffer (50mM Tris-HCl pH7.5, 150mM NaCl, 1% Igepal, 0.5% sodium deoxycholate, 0.1% SDS, 500uM DTT) with proteases inhibitors. Twenty µg of whole cell lysate were loaded in Novex WedgeWell 4-20% Tris-Glycine Gel (Invitrogen) and separated through gel electrophoresis (SDS-PAGE) Tris-Glycine-SDS buffer (Invitrogen). The proteins were then transferred to ImmunBlot PVDF membranes (ThermoFisher) for antibody probing. Membranes were incubated with 10% BSA in TBST for 30 minutes at room temperature (RT), then incubated for variable times with the suitable antibodies diluted in 5% BSA in 1X TBST, washed with TBST and incubated with a dilution of 1:10000 of secondary antibody for one hour at RT. The antibody was then visualized using Super Signal West Dura Extended Duration Substrat (ThermoFisher) and imaged with Amersham Imager 680.

**Cell fractionation**

$5 \times 10^6$cells/condition were collected and suspended in E1 buffer (50mM HEPES-KOH, 140mM NaCl, 1mM EDTA, 10% glycerol, 0.5% NP-40, 0.25% Triton X-100, 1mM DTT, 1X Proteinase Inhibitor) followed by a centrifugation step of 1100 g at 4°C for 2min. The cytoplasmic fraction was collected in a fresh tube. Cells were washed two more times with E1 buffer. Pellet was subsequently suspended in E2 buffer (10mM Tris-HCl, 200mM NaCl, 1mM EDTA, 0.5mM EGTA, 1X Proteinase Inhibitor) followed by a centrifugation step of 1100 g at 4°C for 2 min. Nuclear fraction was collected in a fresh tube. Cells were washed two more times with E2 buffer. After the third wash, pellet was suspended in E3 buffer (500mM Tris-HCl, 500mM NaCl, 1X Proteinase Inhibitor) and sonicated for 15 sec (5 sec ON/ 5 sec OFF). Cytoplasmic, nuclear and chromatin fraction were centrifuge at 16000 g for 10min at 4°C.

**Antibodies**

ARID1B ChIP-Seq: Abcam ab57461. ARID1B western blot: Santa-Cruz sc-32762 and Abcam ab57461. ARID1A ChIP-Seq: GeneTex GTX129433. ARID1A western blot: Cell Signaling Technologies 12354S. Beta-Actin western blot: Cell Signaling Technologies 8457P. SOX2 ChIP-Seq: Active Motif 39843. NANOG ChIP-Seq: R&D Systems AF1997. H3K27ac ChIP-Seq: Abcam ab4729. GAPDH western blot: Cell Signaling Technologies 5174T. CD10 Flow Cytometry: Miltenyi Biotech 130-124-262. CD99 Flow Cytometry: Miltenyi Biotech 130-121-086. SSEA4 Flow Cytometry: Biolegend 330417. TRA-1-60-R Flow Cytometry: Biolegend 330609. IgG ChIP-qPCR: Cell Signaling Technologies 2729S. Cell Signaling HRP-conjugated anti-rabbit (7074S) and anti-mouse (7076S) were used as secondary antibodies in western blot. Spike-in Antibody: Active Motif 61686. Spike-in Chromatin: Active Motif 53083. Antibodies used in immunofluorescence:

670 Anti-Mouse OCT4 (STEMCELL TECHNOLOGIES, 60059, 1:200); Rabbit Monoclonal Anti-Sox9 (abcam,
671 ab185230,1:250); pPolyclonal Goat Anti-Nanog (R&D System, AF1997-SP,1:20); donkey anti-goat IgG
672 (H+L) Alexa 488 (Jackson ImmunoResearch, 705-545-003, 1:500); donkey anti-mouse IgG (H+L) Alexa 647
673 (Jackson ImmunoResearch, 715-605-150, 1:500); Donkey anti-rabbit IgG (H+L) Cy3 (Jackson
674 ImmunoResearch, 11-165-152, 1:500). , Monoclonal mouse anti-human TRA-1-60 Antibody (Millipore
675 MAB4360C3,1:100), Monoclonal mouse Anti-Stage-Specific Embryonic Antigen-4 Antibody (Millipore,
676 MAB4304,1:100), Polyclonal Goat Anti- Human/Mouse Oct-3/4 Antibody (R&D System, AF1759,1:20).
677
678 **Immunofluorescence**
679 Upon fixation (4% PFA for 10 minutes), cells were permeabilized in blocking solution (0.1% Triton X-100,
680 re PBS, 5% normal donkey serum) and then incubated with the antibody of interest. The total number of
681 cells in each field was determined by counterstaining cell nuclei with 4,6-diamidine-2-phenylindole
682 dihydrochloride (DAPI; Sigma-Aldrich; 50 mg/ml in PBS for 15 min at RT). Immunostained cells were
683 mounted in Aqua-Poly/Mount (Polysciences) and analyzed at epi-fluorescent or confocal microscopy,
684 using a Nikon A1R+. Images were captured with a ×40 objectives and a pinhole of 1.2 Airy unit. Analyses
685 were performed in sequential scanning mode to rule out cross-bleeding between channels.
686
687 **Real-time quantitative polymerase chain reaction (RT-qPCR)**
688 Cells were lysed in Tri-reagent and RNA was extracted using the Direct-zol RNA MiniPrep kit (Zymo
689 research). 600ng of template RNA was retrotranscribed into cDNA using RevertAid first strand cDNA
690 synthesis kit (Thermo Scientific) according to manufacturer directions. 15ng of cDNA were used for each
691 real-time quantitative PCR reaction with 0.1 µM of each primer, 10 µL of PowerUp™ SYBR™ Green Master
692 Mix (Applied Biosystems) in a final volume of 20 µl, using QuantStudio 3 Real-Time PCR System (Applied
693 Biosystem). Thermal cycling parameters were set as following: 3 minutes at 95°C, followed by 40 cycles of
694 10 s at 95°C, 20 s at 63°C followed by 30 s at 72°C. Each sample was run in triplicate. 18S rRNA was used
695 as normalizer. Primer sequences are reported in Supplementary Table S1.
696
697 **ChIP-Seq and ChiP-qPCR**
698 Samples from different conditions were processed together to prevent batch effects.
699 For SOX2, NANOG and H3K27ac, for each replicate, 10 million cells were cross-linked with 1%
700 formaldehyde for 5 min at room temperature, quenched with 125mM glycine, harvested and washed
701 twice with 1× PBS. The pellet was resuspended in ChIP lysis buffer (150 mM NaCl, 1% Triton X-100, 0,7%
702 SDS, 500 µM DTT, 10 mM Tris-HCl, 5 mM EDTA) and chromatin was sheared to an average length of 200–
703 500 bp, using a Covaris S220 Ultrasonicator. The chromatin lysate was diluted with SDS-free ChIP lysis
704 buffer. For ChIP-seq, 10 µg of antibody (3 µg for H3K27ac) was added to 5 µg of sonicated chromatin along
705 with Dynabeads Protein A magnetic beads (Invitrogen) and incubated at 4 °C overnight. For SOX2 and
706 NANOG ChIP-seq, 10 ng of spike-in Drosophila chromatin (Active Motif) was added to each sample with
707 2 µg spike-in antibody (Active Motif). On day 2, beads were washed twice with each of the following
708 buffers: Mixed Micelle Buffer (150 mM NaCl, 1% Triton X-100, 0.2% SDS, 20 mM Tris-HCl, 5 mM EDTA,
709 65% sucrose), Buffer 500 (500 mM NaCl, 1% Triton X-100, 0.1% Na deoxycholate, 25 mM HEPES, 10 mM
710 Tris-HCl, 1 mM EDTA), LiCl/detergent wash (250 mM LiCl, 0.5% Na deoxycholate, 0.5% NP-40, 10 mM Tris-
711 HCl, 1 mM EDTA) and a final wash was performed with 1× TE. Finally, beads were resuspended in 1× TE
712 containing 1% SDS and incubated at 65 °C for 10 min to elute immunocomplexes. Elution was repeated
713 twice, and the samples were further incubated overnight at 65 °C to reverse cross-linking, along with the
714 untreated input (5% of the starting material). On day 3, after treatment with 0.5 mg/ml Proteinase K for
715 1h at 65 °C, DNA was purified with Zymo ChIP DNA Clear Concentrator kit and quantified with QUBIT.
716 For ARID1A and ARID1B ChIP-Seq, 10 million cells were cross-linked with EGS (150 mM) for 30min at room
717 temperature followed by a second cross-link with 1% formaldehyde for 15 min at room temperature. The

718 formaldehyde was quenched with by adding glycine (0.125M) for 10 min at room temperature. Cells were
719 washed twice with 1× PBS. Pellet was resuspended in buffer LB1 (50 mM Hepes-KOH, 140 mM NaCl, 1 mM
720 EDTA, 10% Glycerol, 0.5% NP-40, 0.255 Triton X-100), incubated 10 min at 4 °C followed by a
721 centrifugation step of 600g for 5 min at 4 °C. Pellet was suspended in buffer LB2 (10 mM Tris-HCl, 20 mM
722 NaCl, 1 mM EDTA, 0.5 mM EGTA) incubated 10 min at 4 °C followed by a centrifugation step of 600g for 5
723 min at 4 °C. Cells were then resuspended in buffer LB3 (10 mM Tris-HCl, 200 mM NaCl, 1mM EDTA, 0.5
724 mM EGTA, 0.1% Na-DOC, 0.5% N-laurosylsarcosine) incubated 10 min at 4 °C followed by a centrifugation
725 step of 600g for 5min at 4 °C. Pellet was suspended in LB3 and chromatin was sheared to an average
726 length of 200–500 bp, using a Covaris S220 Ultrasonicator. For each sample, 15 ug of sonicated chromatin
727 was incubated at 4 °C overnight along with Dynabeads Protein G conjugated with 10ug of antibody. On
728 day 2, beads were washed once with each of the following buffers: WB1 (50 mM Tris-HCl, 150 mM NaCl,
729 0.15 SDS, 0.1% Na-DOC, 1% Triton X-100, 1 mM EDTA), WB2 (50 mM Tris-HCl, 500 mM NaCl, 0.15 SDS,
730 0.1% Na-DOC, 1% Triton X-100, 1 mM EDTA), WB3 (10 mM Tris-HCl, 250 mM LiCL, 0.55 NP-40. 0.55 Na-
731 DOC, 1 mM EDTA), TE Buffer (10 mM Tris-HCl, 1mM EDTA). Finally, beads were resuspended in EB (10 mM
732 tris-HCl, 0.55 SDS, 300 mM NaCl, 5mM EDTA) and incubated at 65 °C for 30 min to elute
733 immunocomplexes. Elution was repeated twice, and the samples were further incubated overnight at 65
734 °C to reverse cross-linking, along with the untreated input (5% of the starting material). On day 3, after
735 treatment with 0.5 mg/ml Proteinase K for 1h at 65 °C.
736 For all ChIP-seq experiments, barcoded libraries were made with NEB ULTRA II DNA Library Prep Kit for
737 Illumina, and sequenced on Illumina NextSeq 500, producing 75bp SE reads.
738 For ChIP-qPCR, on day 1 the sonicated lysate was aliquot into single immunoprecipitations of $2.5 \times 10^6$
739 cells each. A specific antibody or a total rabbit IgG control was added to the lysate along with Protein A
740 magnetic beads (Invitrogen) and incubated at 4 °C overnight. On day3, ChIP eluates and input were
741 assayed by real-time quantitative PCR in a 20 µl reaction with the following: 0.4 µM of each primer, 10 µl
742 of PowerUp SYBR Green (Applied Biosystems), and 5 µl of template DNA (corresponding to 1/40 of the
743 elution material) using the fast program on QuantStudio qPCR machine (Applied Biosystems). Thermal
744 cycling parameters were: 20sec at 95 °C, followed by 40 cycles of 1sec at 95°C, 20sec at 60°C.
745
746 **ChIP-seq Analyses**
747 After removing the adapters, the sequences were aligned to the reference hg19, using Burrows Wheeler
748 Alignment tool (BWA), with the MEM algorithm[64] . Aligned reads were filtered based on mapping quality
749 (MAPQ > 10) to restrict our analysis to higher quality and likely uniquely mapped reads, and PCR duplicates
750 were removed. We called peaks for each individual using MACS2[65] (H3K27ac) or Homer[66], at 5% FDR, with
751 default parameters.
752
753 **RNA-Seq**
754 Cells were lysed in Tri-reagent (Zymo research) and total RNA was extracted using Quick-RNA Miniprep
755 kit (Zymo research) according to the manufacturer's instructions. RNA was further quantified using
756 DeNovix DS-11 Spectrophotometer while the RNA integrity was checked on Bioanalyzer 2100 (Agilent).
757 Only samples with RIN value above 8.0 were used for transcriptome analysis. RNA libraries were prepared
758 using 1 µg of total RNA input using NEBNext® Poly(A) mRNA Magnetic Isolation Module, NEBNext®
759 UltraTM II Directional RNA Library Prep Kit for Illumina® and NEBNext® UltraTM II DNA Library Prep Kit for
760 Illumina® according to the manufacturer's instructions (New England Biolabs).
761
762 **RNA-Seq Analyses**
763 Reads were aligned to hg19 using STAR v2.5[67], in 2-pass mode with the following parameters: --
764 quantMode TranscriptomeSAM --outFilterMultimapNmax 10 - -outFilterMismatchNmax 10 --
765 outFilterMismatchNoverLmax 0.3 --alignIntronMin 21 -- alignIntronMax 0 --alignMatesGapMax 0 --

766 alignSJoverhangMin 5 --runThreadN 12 -- twopassMode Basic --twopass1readsN 60000000 --
767 sjdbOverhang 100. We filtered bam files based on alignment quality (q = 10) using Samtools v0.1.19[64]. We
768 used the latest annotations obtained from Ensembl to build reference indexes for the STAR alignment.
769 Kallisto[68] was used to count reads mapping to each gene. RSEM[69] was instead used to obtain FPKM
770 (Fragments Per Kilobase of exon per Million fragments mapped). We analyzed differential gene expression
771 levels with DESeq2[70], with the following model: design = ~condition, where condition indicates either CTRL
772 or Patients.
773
774 **ATAC-Seq**
775 For ATAC-Seq experiments, 50,000 cells per condition were processed as described in the original ATAC-
776 seq protocol paper[71]. ATAC-seq data were processed with the same pipeline described for ChIP-seq, with
777 one modification: all mapped reads were offset by +4 bp for the forward-strand and -5 bp for the reverse-
778 strand. After peak calling (MACS2), peaks replicated in all 4 lines (hereafter consensus peaks) were used
779 for downstream analyses.
780
781 **Nuclear extract, IP and LC-MS/MS**
782 After collection, cells were washed twice with ice cold PBS before resuspension in co-IP buffer (20mM Tris
783 pH 7.9, 100mM NaCl, 0.1% NP-40, 0.5mM DTT, protease inhibitors), and rotated for 5 minutes at 4°C.
784 After spinning down at 2000rpm for 10 minutes, the nuclear pellet was resuspended in buffer C (20mM
785 Tris pH 8.0, 1.5mM MgCl2, 0.42M NaCl, 25% glycerol, 0.2mM EDTA, 0.5mM DTT, protease inhibitors),
786 dounce homogenized (with B pestle), and incubated at 4°C for 30 minutes. The extract was centrifuged at
787 12,000rpm for 30 minutes, and the supernatant was kept as nuclear extract. The nuclear extract was
788 dialyzed overnight in BC80 (20mM Tris pH 8.0, 80mM KCl, 0.2mM EDTA, 10% glycerol, 1mM B-
789 mercaptoethanol, 0.2mM phenylmethylsulfonyl fluoride (PMSF)), cleared, and stored at -80°C. For the IP,
790 1.5mg of nuclear extract was incubated for 3 hours at 4°C with 6µg ARID1B antibody and 50µL of
791 Dynabeads Protein A, and the control IP was performed with 0.75mg of nuclear extract and 25µL of
792 Dynabeads Protein A. Beads were washed three times with co-IP buffer, followed by a final wash with
793 0.05% NP-40 in PBS. Elution was performed by agitation in 0.1M glycine pH 3.0 for one minute, and 1M
794 Tris base pH 11.0 was added to neutralize the pH of the eluate. Eluates were prepared for SDS-PAGE and
795 run on a Novex WedgeWell 10% Tris-Glycine Gel (Invitrogen) with Tris-Glycine-SDS buffer (Bio-Rad), at
796 110V for 10 minutes. The gel was stained with Colloidal Blue staining kit (Invitrogen), and further
797 processed at the proteomics facility at the Wistar Institute. Briefly, the gel lanes were excised, reduced
798 with TCEP, alkylated with iodoacetamide, and digested with trypsin. Tryptic digests were analyzed using
799 LC-MS/MS (a standard 90 minute LC gradient on the Thermo Q Exactive HF mass spectrometer). MS/MS
800 spectra were searched with full tryptic specificity against the UniProt human database (10/02/2020) using
801 MaxQuant 1.6.17.0, and also searched for the common protein N-terminal acetylation, Asn deamidation,
802 and Met oxidation. Protein and peptide false discovery rate was set at 1%.
803
804 **Statistical and genomic analyses**
805 All statistical analyses were performed using R v3.3.1. BEDtools v2.27.1[72] was used for genomic analyses.
806 Pathway analysis was performed with Ingenuity Pathway Analysis Suite (QIAGEN Inc.,
807 https://www.qiagenbioinformatics.com/products/ingenuity-pathway-analysis). Motif analyses were
808 performed using the Meme-Suite[73], and specifically with the Meme-ChIP application. Fasta files of the
809 regions of interest were produced using BEDTools v2.27.1. Shuffled input sequences were used as
810 background. E-values < 0.001 were used as threshold for significance[73].
811
812
813 **References**

814 1. Wang, W. *et al.* Purification and biochemical heterogeneity of the mammalian SWI-SNF
815 complex. *EMBO J* **15**, 5370-82 (1996).
816 2. Braun, S.M.G. *et al.* BAF subunit switching regulates chromatin accessibility to control cell
817 cycle exit in the developing mammalian cortex. *Genes Dev* **35**, 335-353 (2021).
818 3. Lessard, J. *et al.* An essential switch in subunit composition of a chromatin remodeling
819 complex during neural development. *Neuron* **55**, 201-15 (2007).
820 4. Gatchalian, J. *et al.* A non-canonical BRD9-containing BAF chromatin remodeling complex
821 regulates naive pluripotency in mouse embryonic stem cells. *Nat Commun* **9**, 5139 (2018).
822 5. Ho, L. *et al.* An embryonic stem cell chromatin remodeling complex, esBAF, is an essential
823 component of the core pluripotency transcriptional network. *Proc Natl Acad Sci U S A* **106**,
824 5187-91 (2009).
825 6. Ho, L. *et al.* An embryonic stem cell chromatin remodeling complex, esBAF, is essential
826 for embryonic stem cell self-renewal and pluripotency. *Proc Natl Acad Sci U S A* **106**, 5181-
827 6 (2009).
828 7. Alfert, A., Moreno, N. & Kerl, K. The BAF complex in development and disease. *Epigenetics*
829 *Chromatin* **12**, 19 (2019).
830 8. Halgren, C. *et al.* Corpus callosum abnormalities, intellectual disability, speech
831 impairment, and autism in patients with haploinsufficiency of ARID1B. *Clin Genet* **82**, 248-
832 55 (2012).
833 9. Hoyer, J. *et al.* Haploinsufficiency of ARID1B, a member of the SWI/SNF-a chromatin-
834 remodeling complex, is a frequent cause of intellectual disability. *Am J Hum Genet* **90**,
835 565-72 (2012).
836 10. Santen, G.W. *et al.* Mutations in SWI/SNF chromatin remodeling complex gene ARID1B
837 cause Coffin-Siris syndrome. *Nat Genet* **44**, 379-80 (2012).
838 11. Tsurusaki, Y. *et al.* Coffin-Siris syndrome is a SWI/SNF complex disorder. *Clin Genet* **85**,
839 548-54 (2014).
840 12. van der Sluijs, P.J. *et al.* The ARID1B spectrum in 143 patients: from nonsyndromic
841 intellectual disability to Coffin-Siris syndrome. *Genet Med* **21**, 1295-1307 (2019).
842 13. Vergano, S.A., van der Sluijs, P.J. & Santen, G. ARID1B-Related Disorder. in
843 *GeneReviews((R))* (eds. Adam, M.P. *et al.*) (Seattle (WA), 1993).
844 14. Santen, G.W. *et al.* Coffin-Siris syndrome and the BAF complex: genotype-phenotype
845 study in 63 patients. *Hum Mutat* **34**, 1519-28 (2013).
846 15. Wieczorek, D. *et al.* A comprehensive molecular study on Coffin-Siris and Nicolaides-
847 Baraitser syndromes identifies a broad molecular and clinical spectrum converging on
848 altered chromatin remodeling. *Hum Mol Genet* **22**, 5121-35 (2013).
849 16. Wright, C.F. *et al.* Genetic diagnosis of developmental disorders in the DDD study: a
850 scalable analysis of genome-wide research data. *Lancet* **385**, 1305-14 (2015).
851 17. Jung, E.M. *et al.* Arid1b haploinsufficiency disrupts cortical interneuron development and
852 mouse behavior. *Nat Neurosci* **20**, 1694-1707 (2017).
853 18. Ka, M., Chopra, D.A., Dravid, S.M. & Kim, W.Y. Essential Roles for ARID1B in Dendritic
854 Arborization and Spine Morphology of Developing Pyramidal Neurons. *J Neurosci* **36**,
855 2723-42 (2016).
856 19. Shibutani, M. *et al.* Arid1b Haploinsufficiency Causes Abnormal Brain Gene Expression
857 and Autism-Related Behaviors in Mice. *Int J Mol Sci* **18**(2017).

858 20. Smith, A.L., Jung, E.M., Jeon, B.T. & Kim, W.Y. Arid1b haploinsufficiency in parvalbumin-
859 or somatostatin-expressing interneurons leads to distinct ASD-like and ID-like behavior.
860 *Sci Rep* **10**, 7834 (2020).
861 21. Sausen, M. *et al.* Integrated genomic analyses identify ARID1A and ARID1B alterations in
862 the childhood cancer neuroblastoma. *Nat Genet* **45**, 12-7 (2013).
863 22. Mashtalir, N. *et al.* Modular Organization and Assembly of SWI/SNF Family Chromatin
864 Remodeling Complexes. *Cell* **175**, 1272-1288 e20 (2018).
865 23. Inoue, K. *et al.* Molecular mechanism for distinct neurological phenotypes conveyed by
866 allelic truncating mutations. *Nat Genet* **36**, 361-9 (2004).
867 24. Prescott, S.L. *et al.* Enhancer divergence and cis-regulatory evolution in the human and
868 chimp neural crest. *Cell* **163**, 68-83 (2015).
869 25. Liu, X. *et al.* De Novo ARID1B mutations cause growth delay associated with aberrant
870 Wnt/beta-catenin signaling. *Hum Mutat* **41**, 1012-1024 (2020).
871 26. Vasileiou, G. *et al.* Chromatin-Remodeling-Factor ARID1B Represses Wnt/beta-Catenin
872 Signaling. *Am J Hum Genet* **97**, 445-56 (2015).
873 27. Lee, J., Lee, J. & Cho, Y.S. Peroxisome Proliferator-Activated Receptor alpha Agonist and
874 Its Target Nanog Cooperate to Induce Pluripotency. *J Clin Med* **7**(2018).
875 28. Mullen, E.M., Gu, P. & Cooney, A.J. Nuclear Receptors in Regulation of Mouse ES Cell
876 Pluripotency and Differentiation. *PPAR Res* **2007**, 61563 (2007).
877 29. Rajasingh, J. & Bright, J.J. 15-Deoxy-delta12,14-prostaglandin J2 regulates leukemia
878 inhibitory factor signaling through JAK-STAT pathway in mouse embryonic stem cells. *Exp*
879 *Cell Res* **312**, 2538-46 (2006).
880 30. Ellegood, J. *et al.* Neuroanatomy and behavior in mice with a haploinsufficiency of AT-rich
881 interactive domain 1B (ARID1B) throughout development. *Mol Autism* **12**, 25 (2021).
882 31. Dodonova, S.O., Zhu, F., Dienemann, C., Taipale, J. & Cramer, P. Nucleosome-bound SOX2
883 and SOX11 structures elucidate pioneer factor function. *Nature* **580**, 669-672 (2020).
884 32. King, H.W. & Klose, R.J. The pioneer factor OCT4 requires the chromatin remodeller BRG1
885 to support gene regulatory element function in mouse embryonic stem cells. *Elife*
886 **6**(2017).
887 33. Blassberg, R. *et al.* Sox2 levels configure the WNT response of epiblast progenitors
888 responsible for vertebrate body formation. 2020.12.29.424684 (2020).
889 34. Bunina, D. *et al.* Genomic Rewiring of SOX2 Chromatin Interaction Network during
890 Differentiation of ESCs to Postmitotic Neurons. *Cell Syst* **10**, 480-494 e8 (2020).
891 35. Heurtier, V. *et al.* The molecular logic of Nanog-induced self-renewal in mouse embryonic
892 stem cells. *Nat Commun* **10**, 1109 (2019).
893 36. Novo, C.L. *et al.* The pluripotency factor Nanog regulates pericentromeric
894 heterochromatin organization in mouse embryonic stem cells. *Genes Dev* **30**, 1101-15
895 (2016).
896 37. De Kumar, B. *et al.* Dynamic regulation of Nanog and stem cell-signaling pathways by
897 Hoxa1 during early neuro-ectodermal differentiation of ES cells. *Proc Natl Acad Sci U S A*
898 **114**, 5838-5845 (2017).
899 38. Navarro, P. *et al.* OCT4/SOX2-independent Nanog autorepression modulates
900 heterogeneous Nanog gene expression in mouse ES cells. *EMBO J* **31**, 4547-62 (2012).

901 39. Silva, J. *et al.* Nanog is the gateway to the pluripotent ground state. *Cell* **138**, 722-37
902 (2009).
903 40. Gagliardi, A. *et al.* A direct physical interaction between Nanog and Sox2 regulates
904 embryonic stem cell self-renewal. *EMBO J* **32**, 2231-47 (2013).
905 41. Rodda, D.J. *et al.* Transcriptional regulation of nanog by OCT4 and SOX2. *J Biol Chem* **280**,
906 24731-7 (2005).
907 42. Shang, L. *et al.* Mutations in ARID2 are associated with intellectual disabilities.
908 *Neurogenetics* **16**, 307-14 (2015).
909 43. Trizzino, M. *et al.* The Tumor Suppressor ARID1A Controls Global Transcription via Pausing
910 of RNA Polymerase II. *Cell Rep* **23**, 3933-3945 (2018).
911 44. Raab, J.R., Resnick, S. & Magnuson, T. Genome-Wide Transcriptional Regulation Mediated
912 by Biochemically Distinct SWI/SNF Complexes. *PLoS Genet* **11**, e1005748 (2015).
913 45. Lu, J. *et al.* Stem cell factor SALL4 represses the transcriptions of PTEN and SALL1 through
914 an epigenetic repressor complex. *PLoS One* **4**, e5577 (2009).
915 46. Miller, A. *et al.* Sall4 controls differentiation of pluripotent cells independently of the
916 Nucleosome Remodelling and Deacetylation (NuRD) complex. *Development* **143**, 3074-84
917 (2016).
918 47. Tatetsu, H. *et al.* SALL4, the missing link between stem cells, development and cancer.
919 *Gene* **584**, 111-9 (2016).
920 48. Yang, J. *et al.* Genome-wide analysis reveals Sall4 to be a major regulator of pluripotency
921 in murine-embryonic stem cells. *Proc Natl Acad Sci U S A* **105**, 19756-61 (2008).
922 49. Pantier, R. *et al.* SALL4 controls cell fate in response to DNA base composition. *Mol Cell*
923 **81**, 845-858 e8 (2021).
924 50. Kohlhase, J. SALL4-Related Disorders. in *GeneReviews((R))* (eds. Adam, M.P. *et al.*) (Seattle
925 (WA), 1993).
926 51. Pagliaroli, L. & Trizzino, M. The Evolutionary Conserved SWI/SNF Subunits ARID1A and
927 ARID1B Are Key Modulators of Pluripotency and Cell-Fate Determination. *Front Cell Dev*
928 *Biol* **9**, 643361 (2021).
929 52. Zhang, Y. *et al.* A switch from hBrm to Brg1 at IFNgamma-activated sequences mediates
930 the activation of human genes. *Cell Res* **20**, 1345-60 (2010).
931 53. Betschinger, J. *et al.* Exit from pluripotency is gated by intracellular redistribution of the
932 bHLH transcription factor Tfe3. *Cell* **153**, 335-47 (2013).
933 54. Jaenisch, R. & Young, R. Stem cells, the molecular circuitry of pluripotency and nuclear
934 reprogramming. *Cell* **132**, 567-82 (2008).
935 55. Takahashi, K. & Yamanaka, S. A decade of transcription factor-mediated reprogramming
936 to pluripotency. *Nat Rev Mol Cell Biol* **17**, 183-93 (2016).
937 56. Gao, F. *et al.* Heterozygous Mutations in SMARCA2 Reprogram the Enhancer Landscape
938 by Global Retargeting of SMARCA4. *Mol Cell* **75**, 891-904 e7 (2019).
939 57. Ejaz, R., Babul-Hirji, R. & Chitayat, D. The evolving features of Nicolaides-Baraitser
940 syndrome - a clinical report of a 20-year follow-up. *Clin Case Rep* **4**, 351-5 (2016).
941 58. Wolff, D. *et al.* In-Frame Deletion and Missense Mutations of the C-Terminal Helicase
942 Domain of SMARCA2 in Three Patients with Nicolaides-Baraitser Syndrome. *Mol*
943 *Syndromol* **2**, 237-244 (2012).

944 59. Kadoch, C. & Crabtree, G.R. Mammalian SWI/SNF chromatin remodeling complexes and
945 cancer: Mechanistic insights gained from human genomics. *Sci Adv* **1**, e1500447 (2015).
946 60. Mathur, R. *et al.* ARID1A loss impairs enhancer-mediated gene regulation and drives colon
947 cancer in mice. *Nat Genet* **49**, 296-302 (2017).
948 61. Vierbuchen, T. *et al.* AP-1 Transcription Factors and the BAF Complex Mediate Signal-
949 Dependent Enhancer Selection. *Mol Cell* **68**, 1067-1082 e12 (2017).
950 62. Warlich, E. *et al.* Lentiviral vector design and imaging approaches to visualize the early
951 stages of cellular reprogramming. *Mol Ther* **19**, 782-9 (2011).
952 63. Chen, J. *et al.* Rational optimization of reprogramming culture conditions for the
953 generation of induced pluripotent stem cells with ultra-high efficiency and fast kinetics.
954 *Cell Res* **21**, 884-94 (2011).
955 64. Li, H. *et al.* The Sequence Alignment/Map format and SAMtools. *Bioinformatics* **25**, 2078-
956 9 (2009).
957 65. Zhang, Y. *et al.* Model-based analysis of ChIP-Seq (MACS). *Genome Biol* **9**, R137 (2008).
958 66. Heinz, S. *et al.* Simple combinations of lineage-determining transcription factors prime
959 cis-regulatory elements required for macrophage and B cell identities. *Mol Cell* **38**, 576-
960 89 (2010).
961 67. Dobin, A. *et al.* STAR: ultrafast universal RNA-seq aligner. *Bioinformatics* **29**, 15-21 (2013).
962 68. Bray, N.L., Pimentel, H., Melsted, P. & Pachter, L. Near-optimal probabilistic RNA-seq
963 quantification. *Nat Biotechnol* **34**, 525-7 (2016).
964 69. Li, B. & Dewey, C.N. RSEM: accurate transcript quantification from RNA-Seq data with or
965 without a reference genome. *BMC Bioinformatics* **12**, 323 (2011).
966 70. Love, M.I., Huber, W. & Anders, S. Moderated estimation of fold change and dispersion
967 for RNA-seq data with DESeq2. *Genome Biol* **15**, 550 (2014).
968 71. Buenrostro, J.D., Giresi, P.G., Zaba, L.C., Chang, H.Y. & Greenleaf, W.J. Transposition of
969 native chromatin for fast and sensitive epigenomic profiling of open chromatin, DNA-
970 binding proteins and nucleosome position. *Nat Methods* **10**, 1213-8 (2013).
971 72. Quinlan, A.R. & Hall, I.M. BEDTools: a flexible suite of utilities for comparing genomic
972 features. *Bioinformatics* **26**, 841-2 (2010).
973 73. Bailey, T.L. *et al.* MEME SUITE: tools for motif discovery and searching. *Nucleic Acids Res*
974 **37**, W202-8 (2009).
975

FIGURE 1

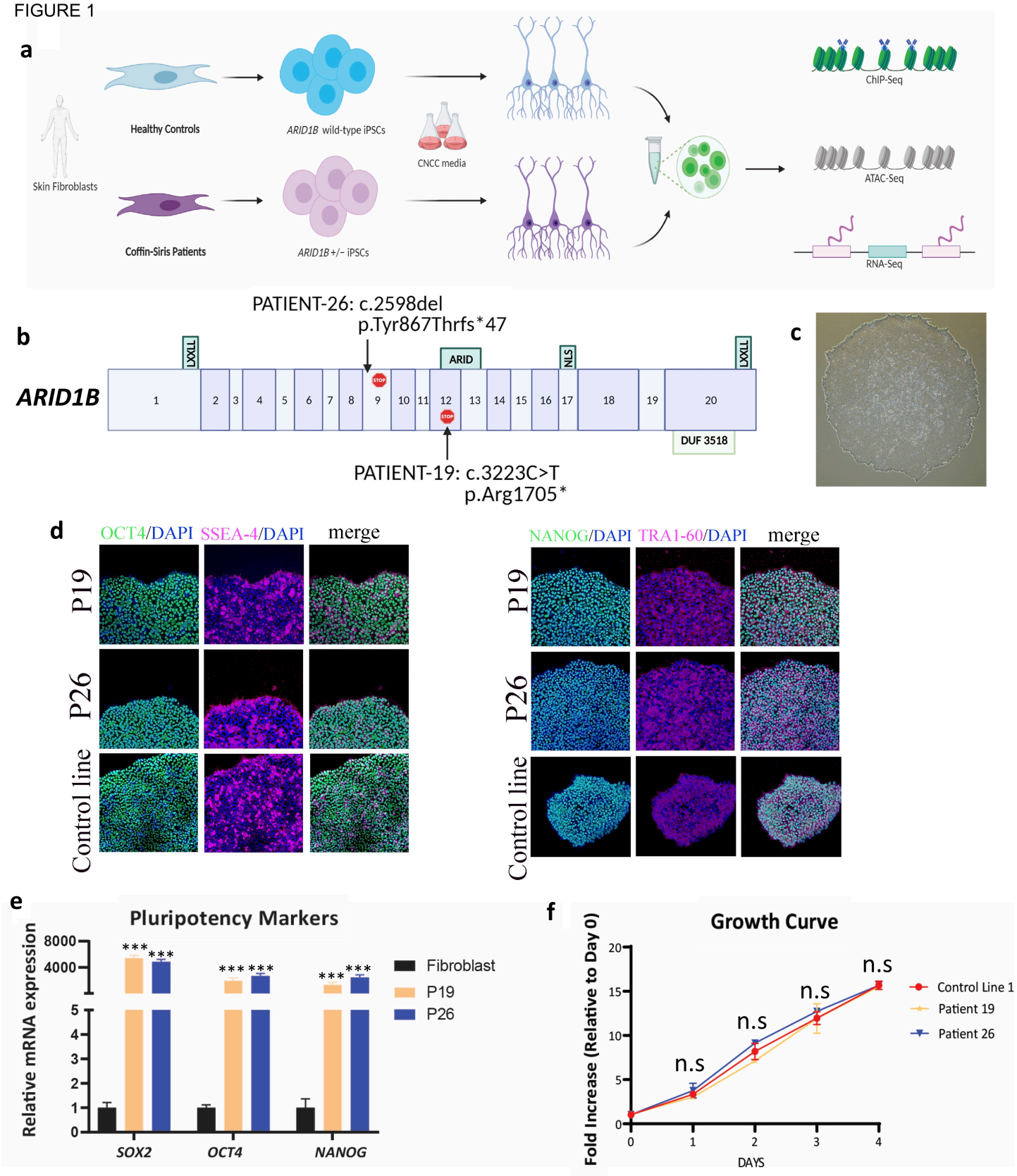
a
Skin Fibroblasts
Healthy Controls
ARID1B wild-type iPSCs
CNCC media
Coffin-Siris Patients
ARID1B +/- iPSCs
ChIP-Seq
ATAC-Seq
RNA-Seq
b
ARID1B
PATIENT-26: c.2598del
p.Tyr867Thrfs*47
LXXLL
ARID
NLS
LXXLL
STOP
DUF 3518
PATIENT-19: c.3223C>T
p.Arg1705*
c
d
OCT4/DAPI
SSEA-4/DAPI
merge
NANOG/DAPI
TRA1-60/DAPI
merge
P19
P26
Control line
e
Pluripotency Markers
Relative mRNA expression
Fibroblast
P19
P26
SOX2
OCT4
NANOG
f
Growth Curve
Fold Increase (Relative to Day 0)
DAYS
Control Line 1
Patient 19
Patient 26
n.s

FIGURE 2

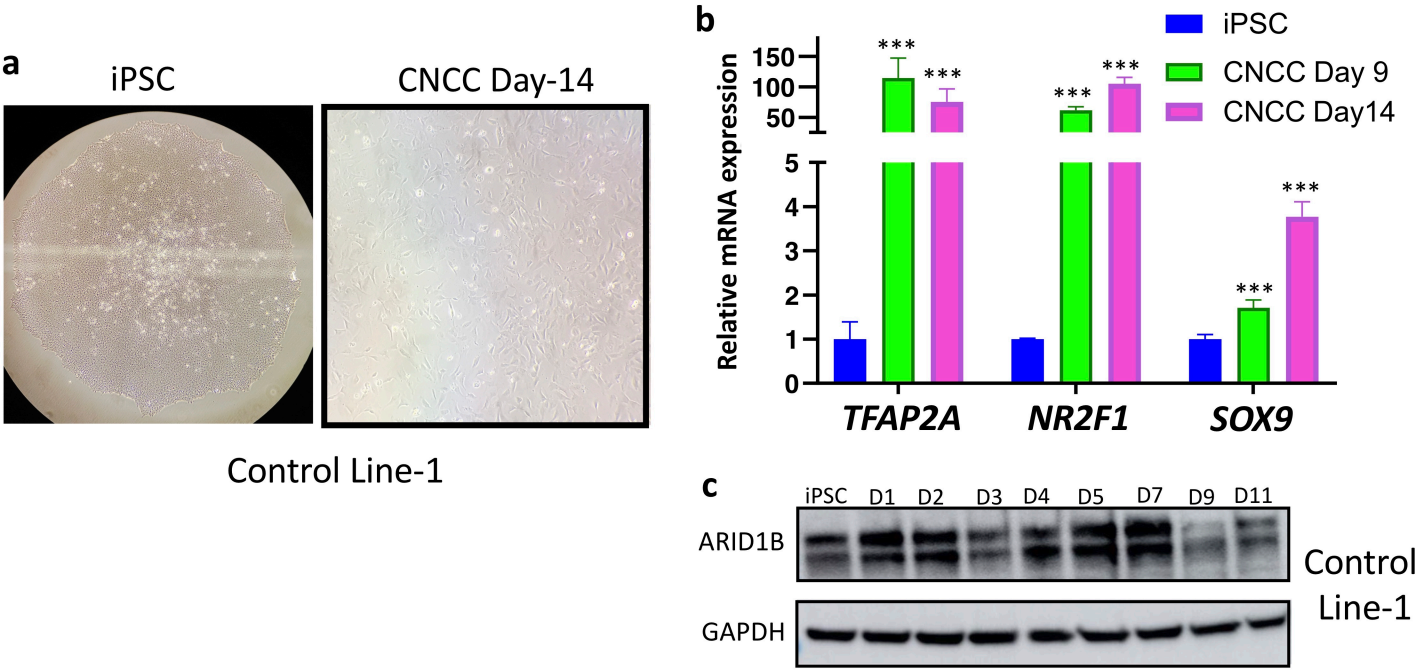
a
iPSC
CNCC Day-14
Control Line-1
b
iPSC
CNCC Day 9
CNCC Day14
Relative mRNA expression
150
100
50
5
4
3
2
1
0
***
TFAP2A
NR2F1
SOX9
c
iPSC D1 D2 D3 D4 D5 D7 D9 D11
ARID1B
GAPDH
Control Line-1

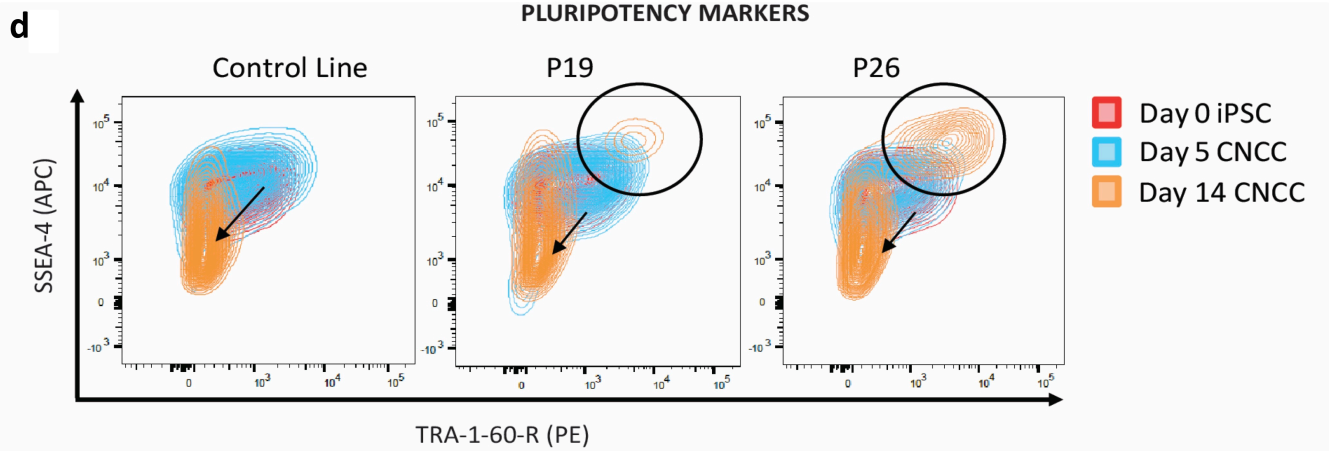
d
PLURIPOTENCY MARKERS
Control Line
P19
P26
SSEA-4 (APC)
TRA-1-60-R (PE)
Day 0 iPSC
Day 5 CNCC
Day 14 CNCC

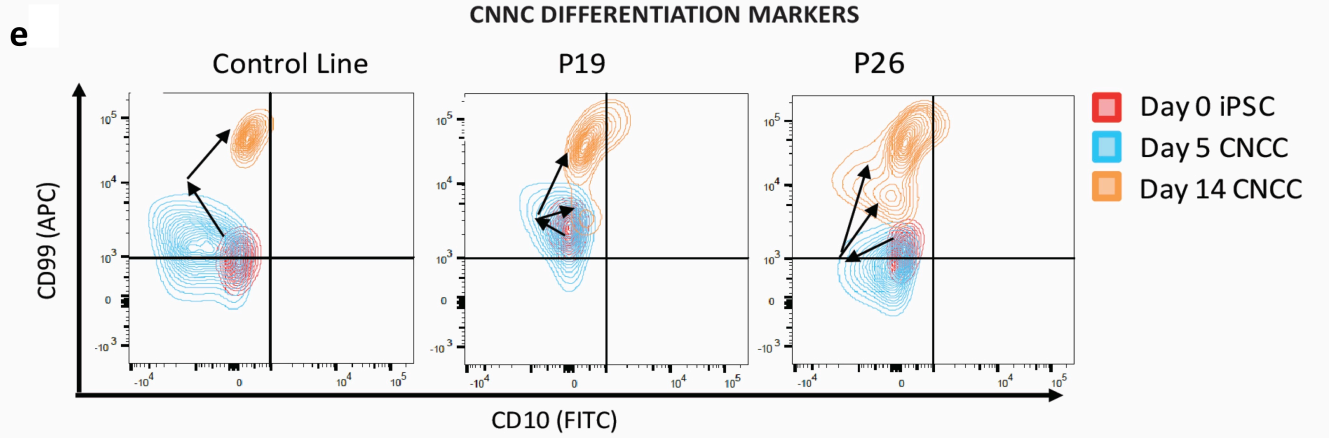
e
CNNC DIFFERENTIATION MARKERS
Control Line
P19
P26
CD99 (APC)
CD10 (FITC)
Day 0 iPSC
Day 5 CNCC
Day 14 CNCC

Figure 1

FIGURE 4

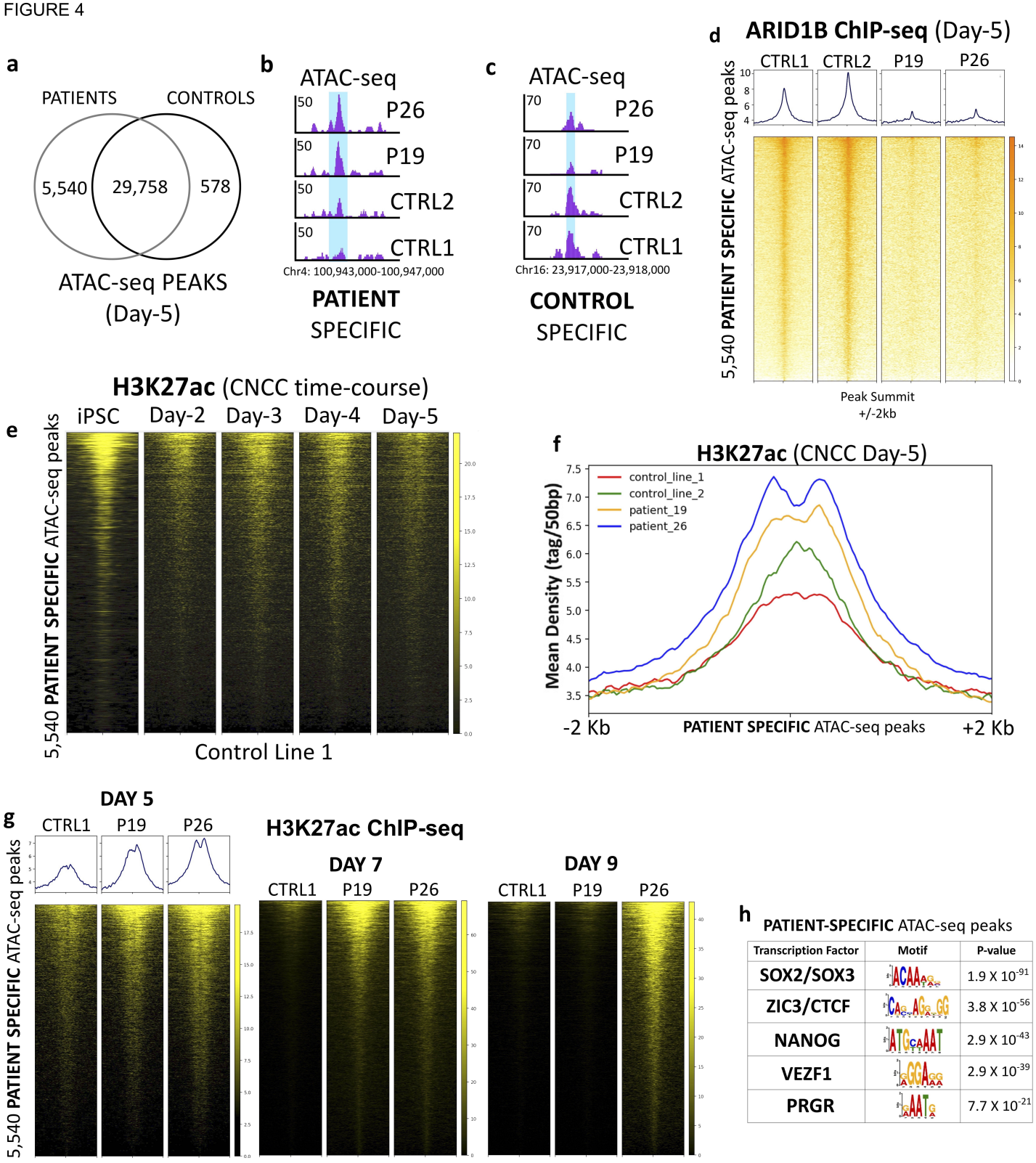


| Transcription Factor | Motif | P-value |
|---|---|---|
| SOX2/SOX3 | | $1.9 \times 10^{-91}$ |
| ZIC3/CTCF | | $3.8 \times 10^{-56}$ |
| NANOG | | $2.9 \times 10^{-43}$ |
| VEZF1 | | $2.9 \times 10^{-39}$ |
| PRGR | | $7.7 \times 10^{-21}$ |

FIGURE 5

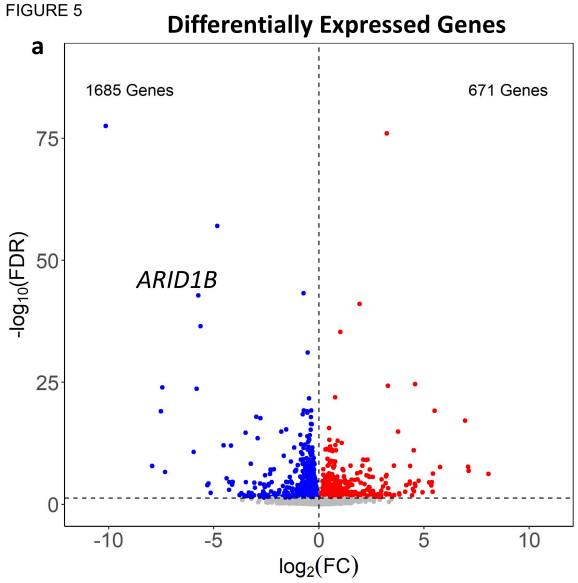


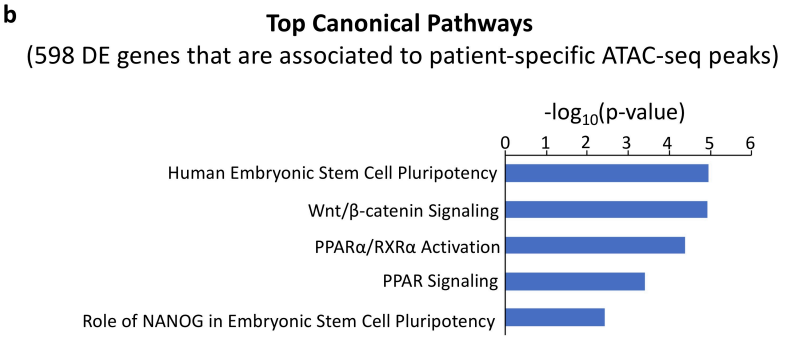


c

| Top Upstream Regulators (598 genes) | |
|---|---|
| FOS | $p = 1.54 \times 10^{-10}$ |
| SOS | $p = 4.68 \times 10^{-9}$ |
| **SOX2** | $p = 4.73 \times 10^{-6}$ |
| TGFB1 | $p = 2.07 \times 10^{-5}$ |
| PRL | $p = 2.64 \times 10^{-5}$ |

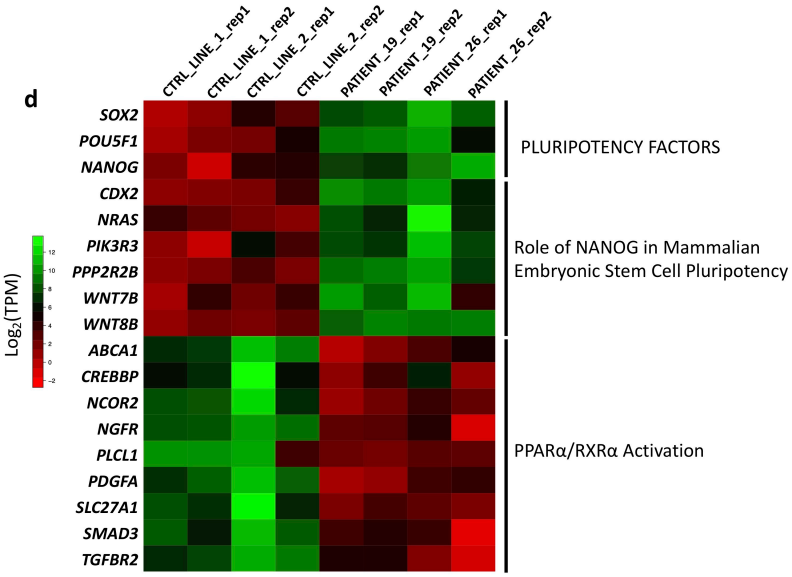

FIGURE 6

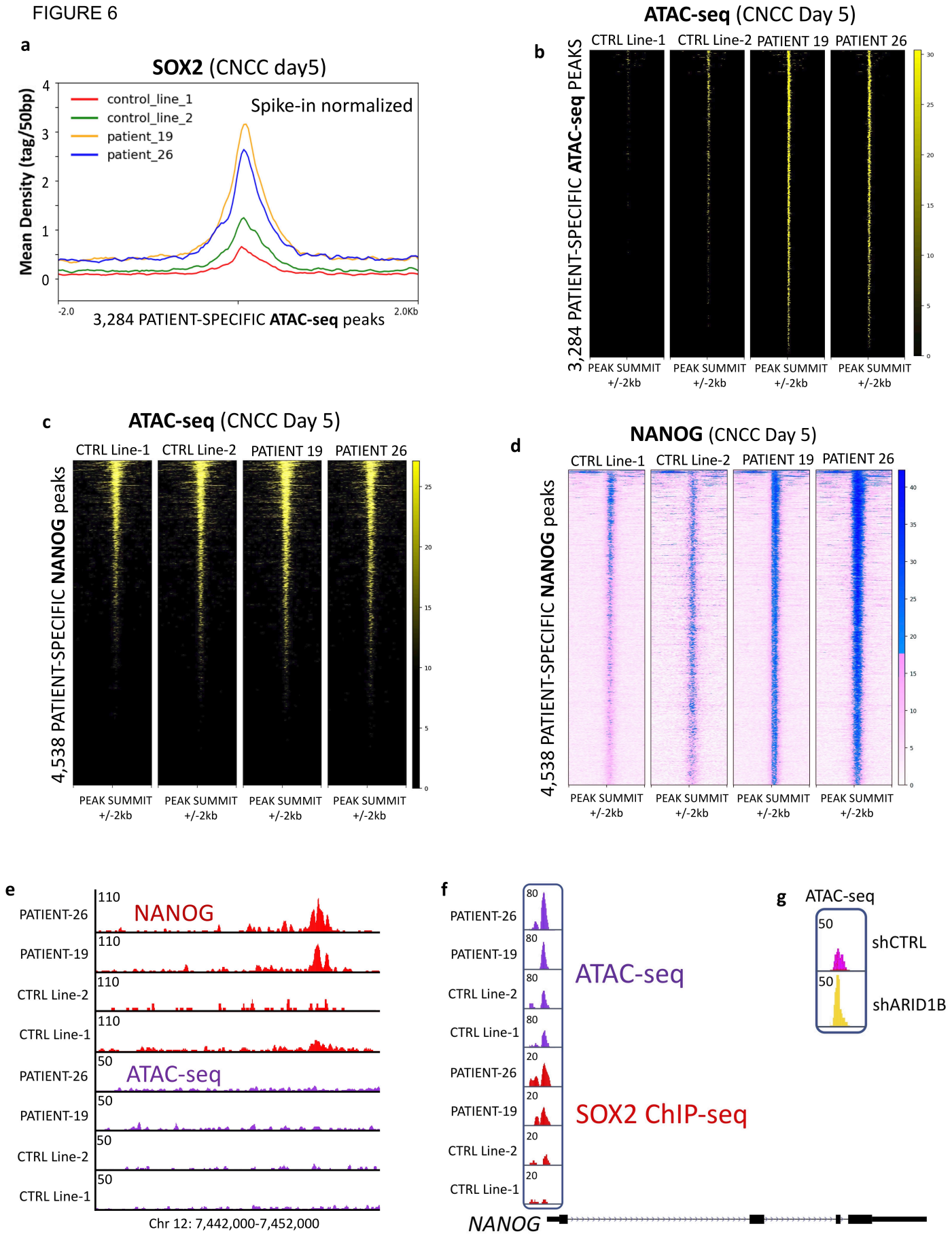
a
SOX2 (CNCC day5)
Spike-in normalized
control_line_1
control_line_2
patient_19
patient_26
Mean Density (tag/50bp)
-2.0
2.0Kb
3,284 PATIENT-SPECIFIC ATAC-seq peaks
b
ATAC-seq (CNCC Day 5)
CTRL Line-1
CTRL Line-2
PATIENT 19
PATIENT 26
3,284 PATIENT-SPECIFIC ATAC-seq PEAKS
PEAK SUMMIT +/-2kb
c
ATAC-seq (CNCC Day 5)
4,538 PATIENT-SPECIFIC NANOG peaks
d
NANOG (CNCC Day 5)
e
NANOG
ATAC-seq
Chr 12: 7,442,000-7,452,000
f
ATAC-seq
SOX2 ChIP-seq
NANOG
g
ATAC-seq
shCTRL
shARID1B

FIGURE 7

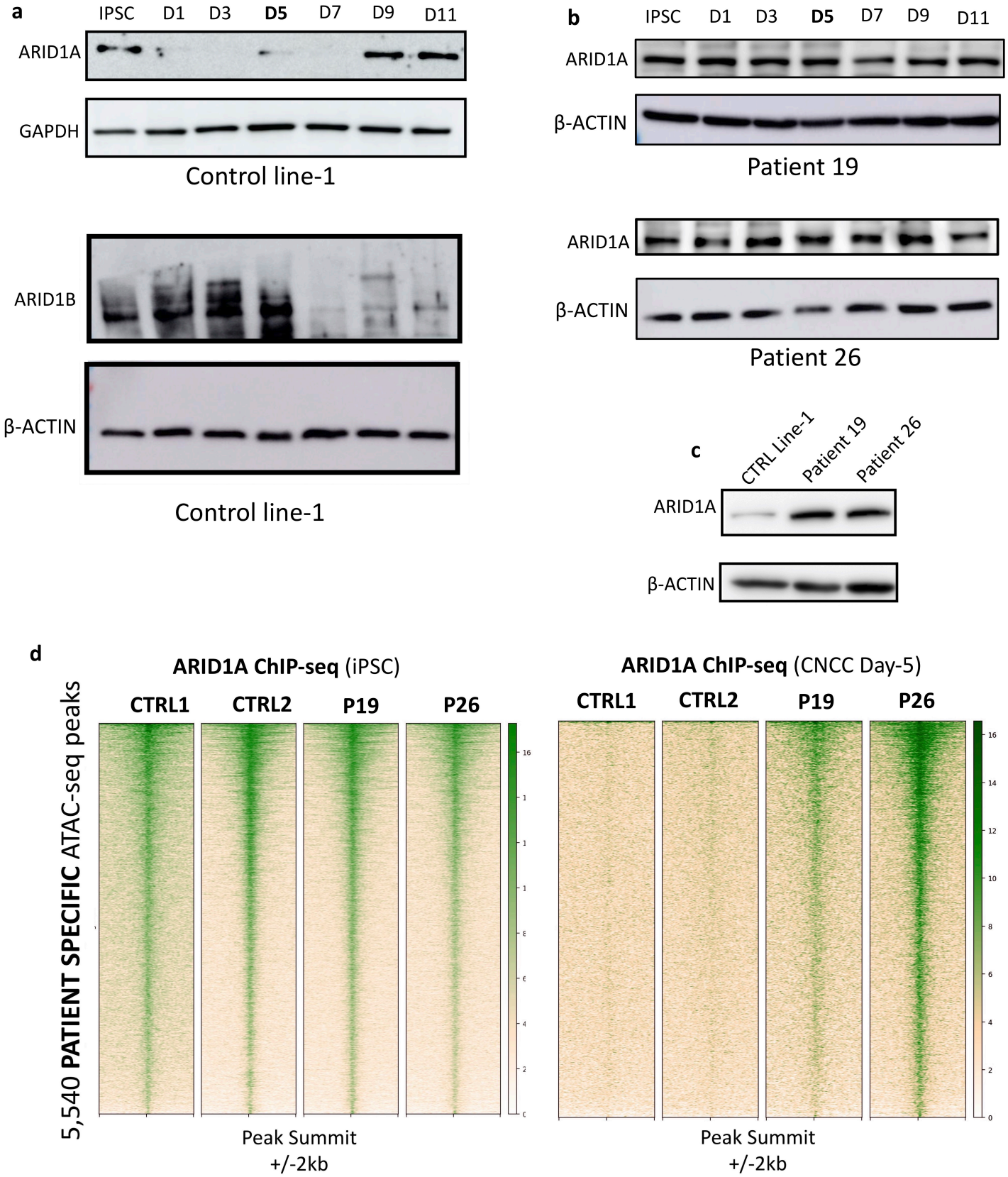
a
IPSC
D1
D3
D5
D7
D9
D11
ARID1A
GAPDH
Control line-1
ARID1B
β-ACTIN
Control line-1
b
IPSC
D1
D3
D5
D7
D9
D11
ARID1A
β-ACTIN
Patient 19
ARID1A
β-ACTIN
Patient 26
c
CTRL Line-1
Patient 19
Patient 26
ARID1A
β-ACTIN
d
ARID1A ChIP-seq (iPSC)
CTRL1
CTRL2
P19
P26
5,540 PATIENT SPECIFIC ATAC-seq peaks
Peak Summit
+/-2kb
ARID1A ChIP-seq (CNCC Day-5)
CTRL1
CTRL2
P19
P26
Peak Summit
+/-2kb